University of Naples "Federico II"

DOCTOR OF PHILOSOPHY, PhD

in Biology

XXIX cycle

2014-2017

CRISPR-Cas9 technology: a new frontier to study *Granulin* gene function in the contest of Neuronal Ceroid Lipofuscinoses 11

Tutor
Prof. Caterina Missero

Co-tutor
Dott. Jlenia Monfregola

Candidate
Dott. Emanuela De Gennaro

TABLE OF CONTENTS

Abbreviations

AAV: Adeno-Associated Viral

ANCL: Adult Neuronal Ceroid Lipofuscinoses

BBB: Blood-Brain Barrier

CLEAR: Coordinated Lysosomal Expression and Regulation

CLN: Ceroid Lipofuscinoses Neuronal

CNS: Central Nervous System

CRISPR: Clustered Regularly Interspaced Short Palindromic Repeats

crRNAs: CRISPR RNAs

CSPα: Cysteine-String Protein α

CTSD: Cathepsin D

CTSF: Cathepsin F

DSB: Double Strand Break

EM: Electron Microscopy

ERT: Enzyme Replacement Therapies

FACS: Fluorescence-Activated Cell Sorting

FDA: Food and Drug Administration

FTD: Frontotemporal Dementia

Gb3: Globotriaosylsphingosine

GFP: Green Fluorescent Protein

GRN: Granulin

HCS: High Content Screening

HDR: Homology Directed Repair

HSC: Haematopoietic Stem Cell

INCL: Infantile Neuronal Ceroid Lipofuscinoses

iPSCs: induced Pluripotent Stem Cells

JNCL: Juvenile Neuronal Ceroid Lipofuscinoses

LAMP1: Lysosomal-Associated Membrane Protein 1

LINCL: Late-Infantile Neuronal Ceroid Lipofuscinoses

LSD: Lysosomal Storage Disease

LV: Lentiviral

mTORC1: mammalian Target Of Rapamycin Complex 1

NCL: Neuronal Ceroid Lipofuscinoses

NHEJ: Non-Homologous End Joining

NMD: Nonsense-Mediated mRNA Decay

NPCs: Neural Progenitor Cells

PAM: Protospacer Adjacent Motif

PGRN: Progranulin

PPT-1: Palmitoyl Protein Thioesterase 1

PTC: Premature Termination Codon

RFP: Red Fluorescent Protein

SLPI: Secretory Leukocyte Protease Inhibitor

ssODNs: single-stranded DNA oligonucleotides

TALENs: Transcription Activator-Like Effector Nucleases

TDP-43: TAR DNA-binding Protein 43

TFEB: Transcription Factor EB

TNF-α: Tumor Necrosis Factor α

TNFR: TNF Receptor

TPP-1: Tripeptidyl Peptidase I

tracrRNA: transactivating CRISPR RNA

WB: Western Blot

ZFNs: Zinc Finger Nucleases

1. Abstract

Progranulin (PGRN) is a growth factor, containing 7.5 tandem repeats of a cysteine-rich motif, encoded by *Granulin (GRN)* gene. Heterozygous mutations of *GRN* are the main cause of Frontotemporal Dementia (FTD), while homozygous mutations lead to Neuronal Ceroid Lipofuscinoses type 11 (NCL11), a Lysosomal Storage Disorder (LSD) showing accumulation of un-degraded proteins and lipids (lipofuscin) inside the lysosomes. The role of *GRN* in regulating lysosomal functions is still unknown and therapies for NCLs are still not available or only aimed to minimize patients' symptoms rather than to stop the disease progression. One of the main limit in understanding the cellular role of *GRN* is the absence of a good cellular model system, which can allow functional studies, as well as High Content Screening (HCS) experiments, in order to find drugs suitable for specific NCL11 therapies. For this reason, during my PhD studies I focused my work on the generation of the $GRN^{-/-}$ and $GRN^{+/-}$ Arpe19 cell lines by CRISPR-Cas9 technology and on a deep characterization of the autophagic-lysosomal phenotype in both *GRN* homozygous and heterozygous conditions. This phenotypic characterization allowed me to highlight differences between these two conditions. Indeed, in absence of PGRN, cells show an enhanced lysosomal and autophagic pathway with impairment of lysosomal function, in contrast to heterozygous condition in which there is a reduction of the autophagic flux with an unchanged number of lysosomes. On the other hand, I found that both in presence of half PGRN amount and in its absence, mTORC1 (mammalian Target Of Rapamycin Complex 1) activity was reduced and that the Transcription Factor EB (TFEB) was located into the nucleus, with a subsequent transcriptional activation of its autophagic-lysosomal target genes. Moreover, due to the low level of variability inside my cell system, I was able to quantify the lysosomal and the autophagic phenotype, by High Content Opera system, demonstrating that this cellular model is a perfect tool to perform screening of Food and Drug Administration (FDA) approved drugs in order to find novel therapeutic strategies for NCL11.

Il gene *Granulin (GRN)* codifica per il fattore di crescita Progranulin (PGRN) contenente 7.5 domini granulinici ricchi in cisteina. Mutazioni in eterozigosi in tale gene sono la principale causa della Frontotemporal Dementia (FTD), mentre mutazioni in omozigosi sono responsabili di una malattia da accumulo lisosomiale (Lysosomal Storage Disorder –LSD) definita Neuronal Ceroid Lipofuscinoses 11 (NCL11), la cui caratteristica è l'accumulo di proteine e lipidi non degradati (lipofuscina) nei lisosomi. Il ruolo di *GRN* nella regolazione delle funzioni lisosomiali è ancora sconosciuto e le attuali terapie per le NCLs sono solo finalizzate a minimizzare i sintomi nei pazienti piuttosto che a bloccare il progredire della malattia. Alla poca conoscenza dei ruoli svolti da *GRN* all'interno della cellula, contribuisce l'assenza di un buon sistema cellulare da utilizzare come modello in studi funzionali ed esperimenti di High Content Screening (HCS) volti alla ricerca di farmaci da utilizzare in specifiche terapie da applicare ai pazienti affetti da NCL11. Allo scopo di risolvere questa mancanza, durante gli studi del dottorato ho incentrato il mio lavoro sulla generazione di linee cellulari (Arpe19) recanti mutazioni nulle in omozigosi ed eterozigosi nel gene *GRN*, mediante la nuova tecnologia CRISPR-Cas9. L'utilizzo di questi modelli mi ha consentito una approfondita caratterizzazione del fenotipo lisosomiale ed autofagico in entrambe le condizioni genetiche. Tale caratterizzazione fenotipica ha evidenziato le differenze tra le due condizioni. Infatti, in assenza della proteina PGRN, le cellule mostrano un aumentato flusso lisosomiale ed autofagico con un danneggiamento della funzione dei lisosomi, al contrario, in condizioni di eterozigosi si osserva una riduzione del flusso autofagico mentre il numero di lisosomi resta invariato. Inoltre ho verificato che sia in cellule $GRN^{-/-}$ che in cellule $GRN^{+/-}$, l'attività di mTORC1 (mammalian Target Of Rapamycin Complex 1) è ridotta e che il fattore di trascrizione EB (TFEB) è localizzato nel nucleo, con la conseguente attivazione trascrizionale dei geni autofagici e lisosomiali da esso regolati. Infine, grazie ai bassi livelli di variabilità del sistema cellulare che ho generato, ho potuto effettuare quantizzazioni, mediante HCS, dei fenotipi autofagici e lisosomiali, dimostrando così che tale sistema cellulare è un perfetto strumento per

effettuare screening di farmaci approvati dalla Food and Drug Administration (FDA) al fine di trovare nuove strategie terapeutiche per la NCL11.

2. Introduction

2.1 Lysosomal Storage Diseases

Lysosomes are cellular organelles discovered by De Duve 60 years ago[1]. Their name comes from a Greek term that means 'digestive body'. Lysosomes play an important role in processes like degradation of macromolecules, homeostasis of the cell, regulation of autophagy, apoptosis and cell death via signal transduction, but also for phagocytosis and antigen presentation. All these processes are involved in inflammation, oncogenesis, neurodegenerative diseases, skin pigmentation and bone biology. Since lysosomes are crucial effectors of multiple cellular functions, lysosomal defects are causative of a group of approximately 50 inherited metabolic disorders called Lysosomal Storage Diseases (LSDs).

LSDs are caused by mutations in genes that regulates lysosomal functions, like catabolic enzymes that are involved in degradation of macromolecules. The substrates of the defective enzymes build up over time, leading to excess cellular storage of these materials and to dysfunction in many tissues like nervous system, eye, bone, muscle, and reticuloendothelial system. Such perturbations of cellular processes ultimately lead to cell death and organ-specific clinical manifestations[2].

LSDs are rare disorders, with an estimated frequency of 1 in 5,000 live births[3]. Severity and age of onset in LSDs depend on different factors such as residual enzyme activity, location of the mutation with respect to the catalytic site, distribution of stored substrates, defective protein expression and other mechanisms that affect the life span of the cells.

The concept of LSDs was developed in 1963 by Hers who was interested in glycogen storage diseases. He noticed that in Pompe disease glycogen was not stored in the cytoplasm but in an organelle surrounded by a membrane. For the first time Hers suggested that glycogen in Pompe disease was stored in

lysosomes[4]. This observation laid the ground for a new classification of the already clinically recognized disorders as “Lysosomal Storage Diseases”.

Most LSDs are caused by deficiency of soluble lysosomal proteins residing in the lumen of the lysosome, a minority is caused by defects in lysosomal membrane proteins and a number of LSDs are caused by the deficiency of non-lysosomal proteins residing in the endoplasmic reticulum, the Golgi apparatus and the endosomal pathway[5].

At the beginning lysosomal diseases were classified based on the storage compound. Clinically this classification is very useful and well accepted. Disorders in which the accumulation of glycosaminoglycan fragments prevails are classified as mucopolysaccharidoses, those dominated by lipid storage as lipidoses. However, in many lysosomal diseases more than one compound accumulates and the stored material is rather heterogeneous. This is the case of a number of lysosomal glycosidases, which are not specific for a certain substrate, but rather for a sugar residue and the stereochemistry of its linkage. This residue and linkage may occur in glycosaminoglycans as well as in lipids, so that a deficiency of the enzyme results in storage of both.

In many other diseases there is a substantial secondary accumulation of compounds that cannot be explained by the specific enzymatic defect. In fact, some gangliosides accumulate secondarily in mucopolysaccharidoses and accumulation of glucosylceramide, the storage compound of Gaucher disease, has been detected in Niemann-Pick Type C disease. From a pathophysiological point of view, the storage of more than just one compound is important since minor storage compounds may play major roles in disease pathogenesis. Thus, from a biochemical point of view, the widely used classification according to the accumulating substrate is not fully systematic[2,5]. For this reason more recently, LSDs have been classified by molecular defects. This subset includes groups of disorders caused by defects in non-enzymatic lysosomal protein, transmembrane protein, lysosomal enzyme protection, post-translational

processing of lysosomal enzymes, trafficking in lysosomal enzymes and polypeptide degradation[6].

LSDs also comprise another group of disorders named “Neuronal Ceroid Lipofuscinoses (NCLs)”. NCLs are grouped in LSDs because of the intracellular storage material, even though distinct characteristics exist. While in the classic LSDs, the deficiency or dysfunction of an enzyme or transporter leads to lysosomal accumulation of specific undegraded substrates or metabolites, accumulating material in NCLs is not a disease-specific substrate, but lysosomal storage can be caused by defects in secondary processes of membrane turnover or altered endosome and/or lysosome trafficking[2,7].

2.2 Neuronal Ceroid Lipofuscinoses

The NCLs, also referred to as Batten Disease, comprise a group of most common inherited, progressive neurodegenerative diseases of childhood[8]. The NCLs were originally classified based on the clinical onset of symptoms to four main forms: infantile (INCL), late-infantile (LINCL), juvenile (JNCL) and adult (ANCL)[9]. The disease clinical features range from early vision problems and/or seizures progressing to mental impairment, seizures of increased severity, progressive loss of sight and motor skills, as well as increasing spasticity. Children reaching the end-stages of the disease become blind, bedridden, spastic, and demented with poorly controlled seizures before expiring in their teens or early twenties[10,11,12]. Pathogenesis of disease leads to accelerated apoptosis[13,14], impaired autophagy, and secondary destructive inflammation. NCLs are characterized by an accumulation of autofluorescent material, composed by fats and proteins (lipofuscin), in body tissues such as brain and retina, and specifically localized into the lysosomes[15,16]. Furthermore, NCLs show accumulation of subunit c of mitochondrial ATP synthase in lysosome-derived organelles although the exact biochemical mechanism of accumulation is unknown[16].

The NCLs are caused by defects in Ceroid-Lipofuscinoses Neuronal (CLN) proteins or *CLN* genes and, to date, 14 distinct genetic variants are recognized (CLN1-CLN14) (Table1). Proteins encoded by the majority of the *CLN* genes (*CLN1*, *CLN2*, *CLN3*, *CLN5*, *CLN7*, *CLN10*, *CLN12*, and *CLN13*) are primarily localized to the lysosome, although some of them are known to have also extralysosomal functions[18,19]. Mutations in the *CLN3* gene cause JNCL and encode for the CLN3 protein, which is localized to Golgi, lipid rafts, plasma membrane and lysosomes. CLN3 protein function is unknown and mutations in this gene lead to altered lysosomal pH, defective arginine transport, and malfunction in transport across lysosomal and vacuolar membranes[20-22]. Another common NCL variant is CLN2 disease, a LINCL, caused by a defective Tripeptidyl Peptidase I (TPP-1) enzyme, which removes tripeptides

from the N-terminal of small polypeptides[23]. Patients affected by lipofuscinoses 1 present mutation in *CLN1* gene and have a defective Palmitoyl Protein Thioesterase 1 (PPT-1) enzyme[24] responsible for the cleavage of palmitate from S-acylated proteins[25]. CLN4 disease is caused by mutations in the *DNAJC5* gene, which encodes for the protein cysteine-string protein α (CSPα)[26]. CSPα plays a role as a chaperone in folding of proteins and in synaptic vesicle exocytosis and endocytosis[27,28]. CLN10 disease is caused by mutation in the cathepsin D gene (*CTSD*, *CLN10*)[18,29]. *CTSD* gene in the physiological state codes for the protein cathepsin D, an aspartyl endopeptidase, which plays several roles in apoptosis. Mutation in the cathepsin F (*CTSF, CLN13*) gene leads to adult-onset NCL, also known as type B Kuf disease[30]. CTSF is a cysteine protease highly expressed in neurons and is shown to be involved in autophagy and proteasomal degradation[18,29]. Very few is known about the functions of proteins encoded by the genes *CLN5−9*, *CLN11*, *CLN12*, and *CLN14*[18,29] as well as the physiological meaning of CLN proteins interactions is still unknown[29].

NCLs are mostly inherited in an autosomal recessive manner, but some patients with the adult variant of NCL show autosomal dominant inheritance[11]. Despite a worldwide distribution pattern, the incidence of NCLs varies depending on geographical location, ranging from 1 in 14,000 people in Iceland to 1 in 67,000 in Italy and Germany[31].

2.2.1 Cellular and animal models of NCLs

Model systems have always been the strategic tool to study the molecular mechanisms underlying human pathologies. Although very few is known about the pathophysiology of NCLs, the basic understanding of the disease processes elucidated so far, has enabled the development of cellular and animal models mimicking the phenotype of deficient *CLN* genes. Most of the cellular models reported in literature are NCL patient lymphoblasts and fibroblasts, neurons derived from animal models of NCL disease[32–37], neuroblastoma cell line SH-

SY5Y knock-down of the *CLN* genes by gene silencing based method[38] and human induced pluripotent stem cells (iPSCs). iPSCs have gained increasing attention thanks to their ability of reproducing genotypic and phenotypic changes observed in human NCL patients.

Table 1. Human neuronal ceroid lipofuscinoses variants

Disease	OMIM	Clinical phenotype	Gene	Gene product
CLN1	256730	Classic infantile, late infantile, juvenile, adult	*CLN1 (PPT1)*	PPT-1
CLN2	204500	Classic late infantile, juvenile	*CLN2 (TPP1)*	TPP-1
CLN3	204200	Juvenile	*CLN3*	CLN3 protein (battenin)
CLN4	162350	Adult autosomal dominant	*CLN4 (DNAJC5)*	DnaJ homologue subfamily C member 5
CLN5	256731	Late infantile variant, juvenile, adult	*CLN5*	Protein CLN5
CLN6	601780	Late infantile variant, adult (Kuf, type A)	*CLN6*	Protein CLN6
CLN7	610951	Late infantile variant, juvenile, adult	*CLN7 (MFSD8)*	Major facilitator superfamily domain-containing protein 8
CLN8	610003	Late infantile variant (epilepsy with mental retardation)	*CLN8*	Protein CLN8
CLN9	-	Juvenile	*CLN9*	Protein CLN9
CLN10	610127	Congenital classic, late infantile, adult	*CLN10 (CTDS)*	Cathepsin D
CLN11	138945	Adult	*CLN11 (GRN)*	Progranulin
CLN12	-	Juvenile, Kufor-Rakeb syndrome	*CLN12 (ATP13A2)*	-
CLN13	-	Adult Kuf type	*CLN13 (CTSF)*	Cathepsin F
CLN14	-	Infantile, progressive myoclonus epilepsy 3	*CLN14 (KCTD7)*	Potassium channel tetramerization domain-containing protein 7

Adapted from Rakheja, D., et al. (2007)

However, iPSCs suffer, like all the models mentioned above, from high degrees of variation between attempts to reprogram a single fibroblast line or between cells derived from different patients, complicating their use in early drug discovery screens[39].

Mice are the most used model organism for investigating NCL pathogenesis and to date there are genetically engineered (CLN1/PPT1, CLN2/TPP1, CLN3, CLN5, CLN11 and CLN10/CTSD), and spontaneous naturally-occurring mice models (CLN6/nclf and CLN8/mnd) which cover all the NCLs forms[40]. Mice models show key pathological features of their human counterparts, including autofluorescent cellular storage and progressive neurodegeneration[41].

Large animal models of the NCLs offer lots of significant advantages over their small model counterparts. Dogs and sheep models bridge the large gap in brain size and anatomy between rodents and human. These large animals have a longer life expectancy, particularly useful in investigations of long-term treatment effects. Furthermore, the clinical progression in larger animals is more comparable to that seen in human patients[39] and, like the human phenotype, these animal models also accumulate subunit c of mitochondrial ATPase[42].

Using such models, a number of promising therapeutic avenues have been developed, such as adeno-associated viral (AAV) and lentiviral (LV)-mediated gene therapies, enzyme replacement therapies (ERT), stem cell therapies, and small molecule therapies[39].

2.2.2 Therapeutic strategies for NCLs

Scientific research is still moving the first steps in investigating NCLs pathophysiology and is far from the discovery of suitable therapies. To date most of the experimental treatments are focused on minimising symptoms, but none have been able to stop the disease progression or significantly improve the quality of patients' life.

Moreover, lysosomal diseases affecting the brain, like NCLs, present significant difficulties for the treatment due to the protection by blood-brain barrier (BBB)[43]. Therapies relying on the correction or replacement of the faulty protein require expression of the corrected protein to be sustained within the brain, without any associated toxicity, for long-term treatment. The historically trialled technique is the peripherally-administered ERT. This therapy is based on the exogenous administration of the required enzyme, which should be internalized by cells from the extracellular space, via a specific receptor-mediated uptake. This approach is only feasible for NCLs caused by defects in soluble lysosomal enzymes (CLN1, 2, 5 and 10). The first LSD successfully treated by ERT was the non-neuropathic Gaucher disease, although the neurological symptoms were not successfully healed[44] because of the BBB[43]. This means that ERT is highly beneficial for the treatment of peripheral symptoms, but does not show clinical benefit for the Central Nervous System (CNS) pathologies. A strategy to avoid inaccessibility of the BBB, is to deliver the enzyme directly to the CNS via the ventricular space or parenchyma, but the long-term effect of repeated administration, the efficiency of delivery to a large brain area such as human one, and the effectiveness of the therapy using neutralising antibodies must be clarified[43].

A promising treatment option for all forms of NCLs is the viral-mediated gene therapy. This approach is based on the use of a LV or AAV particles containing a cDNA codifying the wild type protein. Viral particles are injected into the CNS of patients in order to express the corrected version of the protein in the transduced cells, thereby restoring protein function. The key advantage of gene therapy is the long term effect. This therapy is in fact a permanent treatment that does not require lifelong repeated administrations into the fragile brain, avoiding further damage[43]. Gene therapy strategies rely on a small population of cells receiving the normal copy of the gene. This group of cells over-expresses and secretes the protein, which will be internalized by neighbouring cells[45]. Thus, this approach for the NCLs needs to consider whether the mutated protein is soluble or membrane-bound. CLN1, CLN2, CLN5 and CLN10 are

secreted from cells so they are compatible with such a cross-correction approach. For NCLs deficient in membrane-bound proteins developing a gene therapy is more difficult because a significantly higher proportion of cells must be transduced. Viral mediated therapy is currently unable to deliver protein to all brain regions, resulting in the need for multiple sites of therapeutic injection. This is due to both the size of the human brain and the high level of protection to external influence carried out by BBB.

Replacement of defective protein is not the sole strategy for NCLs treatments. Impaired cell signalling modulation could be useful to restore the normal cellular function alleviating, in this way, disease pathology[43]. In the last years many small molecules, able to restore the normal enzyme activity and to upregulate impaired cell pathways, have been discovered. These compounds include immunosuppressants, pharmacological chaperons, antioxidants and compounds that promote the read-through of premature stop codons[40]. Small molecules therapy provides the advantage of penetrating the BBB, while macromolecules cannot. The BBB is distrupted in most NCLs and this allows therapeutic agents to reach the brain, however, once the normal function is restored, macromolecules become less effective[39,45]. Another strong advantage of small molecule therapy is the non-invasive methods of drug administration, with the possibility of generating oral formulations that represent a charming alternative to invasive surgical procedures.

Another tested treatment for NCLs is the stem cell therapy. It is based on the principle that stem cells, derived from a healthy donor and transplanted in a patient, are able to migrate to the CNS, where they provide the functional missing protein/enzyme and differentiate into the suitable tissue type. Haematopoietic Stem Cell (HSC) transplantation was performed in NCL patients in order to normalise PPT1 activity. This therapy showed limited or no success because PPT1 activity was normalized in circulating peripheral leukocytes, but not in the cerebrospinal fluid[46]. Also Neural Progenitor Cells (NPCs) are useful for NCL therapies. NPCs are able to integrate into the host

CNS upon transplantation and to differentiate into neurons or glia. This type of treatment was tested in mice using NPCs secreting the functional protein in PPT1 deficient mice[40]. Results showed that transplanted cells were able to engraft, migrate throughout the brain and constantly secrete the functional enzyme. PPT1 secreted by the transplanted cells was shown to be internalised by neighbouring cells in a cross-correction protection process, associated with a decrease in autofluorescent storage material[40]. Clinical trials (ClinicalTrials.gov identifier NCT00337636) were carried out for NCL patients displaying a well-advanced stage of disease. Allogenic foetal neural stem cells (HuCNS-SC) were transplanted into two INCL and four LINCL patients. Post-mortem analysis showed evidence of donor cell engraftment and cell migration from the initial transplantation site but many HuCNS-SCs were not able to differentiate into neurons. If cells are only capable of enzyme secretion, but are not able to replace defective neuronal cells, therapy is only useful as neuroprotection in an early stage of disease and is only applicable for soluble protein NCL disease forms[43].

2.3 Granulin gene

2.3.1 Gene and protein structure

Granulin gene (*GRN*) is located on chromosome 17 (17q21) of human genome and is composed by 13 exons[47]. *GRN* encodes for a 593 amino acids precursor protein, progranulin (PGRN), with a predicted molecular weight of 68.5 kDa. PGRN contains a signal sequence and seven and half tandem repeats characterized by a unique 12 cysteine motif, named granulin domain[48]. This motif consists of four pairs of cysteines flanked by two single cysteines at the amino and carboxyl termini (Fig.1) which generate six disulfide bonds holding two parallel stacked β-hairpins[49,50].

Once transcribed, PGRN undergoes maturation during which the signal peptide is cleaved off and the full-lenght protein is glycosylated and secreted as a 98 kDa precursor protein. In the extracellular environment PGRN undergoes proteolysis mediated by proteases which cleave the linker regions between granulin domains releasing ~6kDa peptides, termed granulins[48]. Proceeding from the N-terminal to the C-terminal of PGRN, granulins are called: p (the half "paragranulin" domain), G, F, B, A, C, D, and E (Fig.1). Proteases involved in progranulin cleavage are: neutrophil elastase[51], MMP-12 (matrix metalloproteinase 12, macrophage elastase)[52], MMP-14[53], ADAMTS-7 (a disintegrin and metalloproteinase with thrombospondin motifs 7)[54] and proteinase3 (a neutrophil protease)[55].

2.3.2 Phylogenesis

Thanks to the particular structure of the granulin motif, the identification of *GRN* homologous genes in other species was successful. No homologous genes were found in *Fungi*, whereas one *GRN* gene was discovered in the amoeba *Dictyostelium discoideum,* a primordial organism that dictated the divergence between plant and animal kingdoms. Both the sponge *Oscarella carmela* and the choanoflagellate *Monosiga brevicollis* have *GRN* gene, but, while the first

has most of the classical growth factor signalling, the second does not. These observations suggest that GRN signalling pathway evolved about 1.5 billion years ago before most of other pathways[56].

Many organisms, such as fish and invertebrate organisms present multiple copies of *GRN*, while in mammals there is only one member of the gene family[56]. Four *GRN* genes are present in zebrafish genome: two small forms (zPGRN-1 and zPGRN-2) containing one and half granulin motif, and two genes (zPGRN-A and zPGRN-B) composed by multiple granulin motifs that are co-orthologs of the human gene[57] (Fig.2).

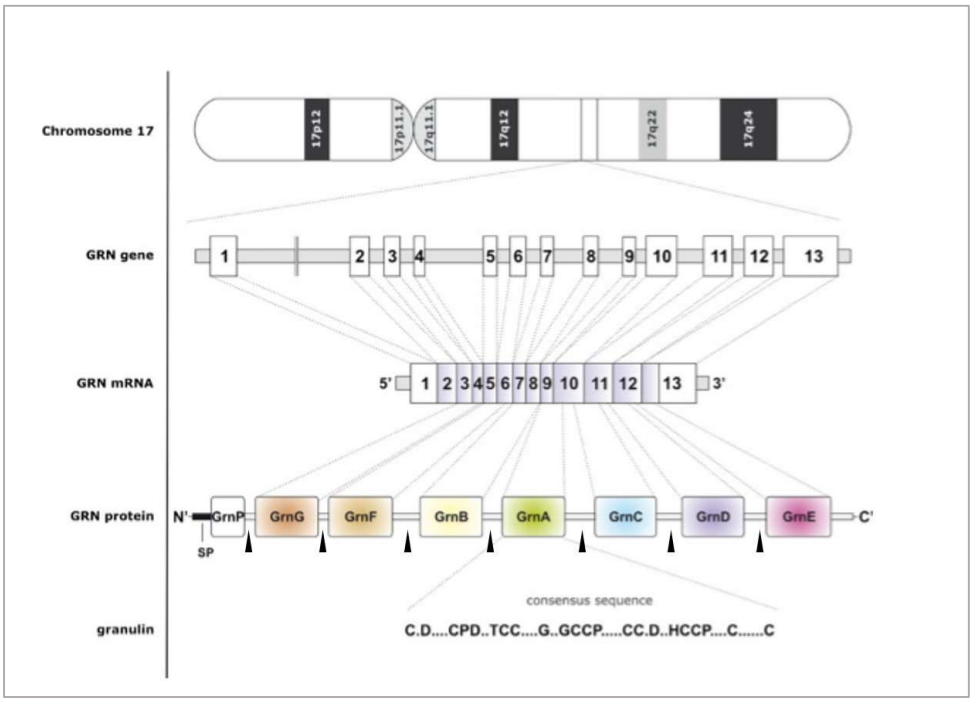

Fig.1 Schematic representation of the *GRN* locus on chromosome 17, the structure of the *GRN* gene, mRNA, protein (PGRN) and consensus amino acid sequence of a granulin domain. Black arrows indicate cleavage sites. (Adapted from Kleinberger G., *et al.* 2013).

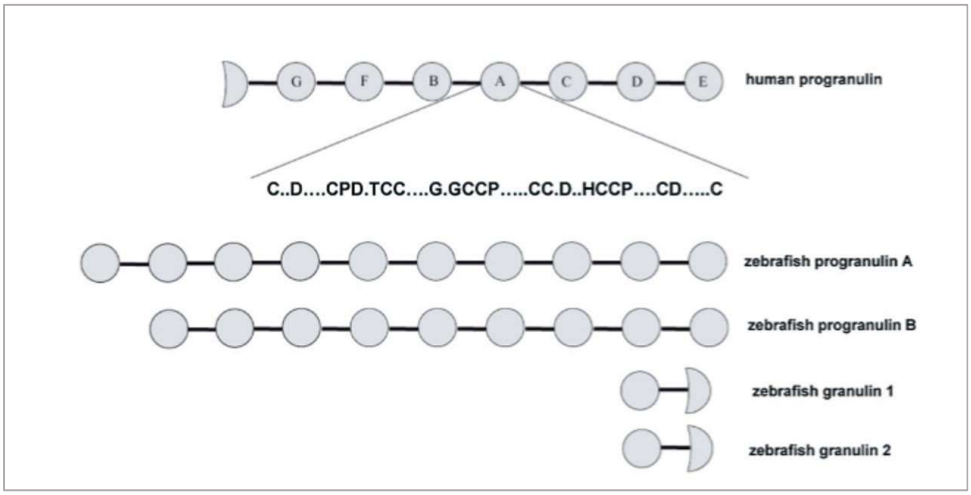

Fig.2 A comparison of the structure of GRN family members in humans and zebrafish. The circles represent the complete granulin modules of 12 cysteines, while semi-circles are partial granulin domains of only six cysteines. (Adapted from Bateman A. and Bennett H.P.J. 2009).

2.3.3 GRN function

Knowledge of *GRN* function is very poor, especially because of the complex and opposite effects of full-length protein and granulin peptides. Published works ascribed to PGRN multiple functions and this is emphasized by the different assignments used in literature: Ceroid-Lipofuscinoses Neuronal 11 (*CLN11*), Granulin-Epithelin Precursor (*GEP*), PC cell-Derived Growth Factor (*PCDGF*), progranulin (*PGRN*), proepithelin (PEPI), acrogranin, epithelial transforming growth factor, 88kDa glycoprotein (GP88)[58-62] (OMIM: 138945).

GRN expression profile spreads through the whole body during development and adulthood. It is expressed particularly in epithelia, immune cells, bone marrow, solid organs like spleen and kidney, and CNS[48,63-68]. In the CNS, *GRN* is expressed in microglia and neurons reaching higher levels, in the first, upon activation, in the second, during maturation[69]. PGRN function in the brain is not completely clear. Recent studies suggest a neuroprotective role of PGRN against premature death in neurons[70] and extracellular administration of PGRN proved an enhanced neurite outgrowth in motor and cortical neurons[71]. Petkau, T. L. *et al*. and Tapia, L. *et al.* demonstrated that depletion of *GRN* in mice[72] and siRNA knockdown in cultured hippocampal neurons[73], lead to a reduced

dendritic length and to an increased number of synaptic vesicles per synapse[73]. This means that the reduction of synaptic connections is balanced by an enhanced transmission at single synapses level[74].

Another important role of PGRN into the brain seems to be its involvement in sexual differentiation. During the embryonic development, the hypothalamus begins a female program of differentiation followed by a masculinization step due to circulating androgens. *GRN* transcriptional levels are upregulated by androgens in neonatal mice and depletion of PGRN showed a reduction in mice masculine behaviour[75,76].

Qin J. *et al* in 2005 published results regarding a role of PGRN in early embryogenesis. PGRN is a growth factor[56] and in the blastocyst it is localized in the trophoblast, the outside cell sheet which, after implantation, will form the fetal compartment of the placenta[77]. After implantation, PGRN continues to be expressed in the placenta[78], in the epidermis and in the developing nervous system of the embryo[66]. This could be correlated with the still unclear role of PGRN in the CNS.

PGRN is expressed in active dividing cells, as in cases of tissue remodelling (embryonic development) and wound healing. In adult epithelia there are high PGRN levels in epidermal keratinocytes and intestinal crypts[65], while in quiescent tissue, like fibroblasts, PGRN levels are lower[63]. In the last one PGRN levels increase considerably during wound healing. In fact, when PGRN was added to the wounds in mouse skin, there was an increasing number of capillaries, neutrophils, macrophages and fibroblasts in the impaired region suggesting a role of PGRN in wound repair[79].

Evidence on PGRN function as a growth factor came from oncological studies reporting an overexpression of PGRN in cancer cells. An increase of PGRN levels was detected in different type of cancers, such as carcinomas[60,80-82], gliomas[83] and sarcomas[84]. Like the activating proliferative pathways of ERK, PI3K and AKT[85-87], PGRN contributes to an aggressive cancer phenotype, making it a suitable anti-cancer treatment target.

Another function ascribed to *GRN* is the regulation of the inflammatory response through the balance of full-length PGRN and granulins. PGRN has a proliferative and anti-inflammatory activity, inhibiting tumor necrosis factor α (TNF-α) signalling[88,89]. The pro-inflammatory granulins A and E are instead able to induce the expression of the cytokines interleukin-8, TNF-α, and interleukin-1b[88,90], triggering the inflammatory response which recruits, in the damaged site, macrophages, neutrophils, blood vessels and fibroblasts during wound healing process[79,88,91]. The balance between full-length PGRN and granulins is regulated by the Secretory Leukocyte Protease Inhibitor (SLPI). SLPI binds PGRN thus preventing the proteolytic cleavage mediated by neutrophil-derived proteases, such as neutrophil elastase and proteinase-3[56].

2.3.4 PGRN receptors

Knowledge of PGRN receptors is actually very poor. The first PGRN receptor was identified by Hu F. *et al.* in 2010[92]. They found a co-localization of PGRN with Sortilin, a single-pass transmembrane protein localized on neurons cell surface. Sortilin is a member of Vps10 protein family and is located in secretory and endocytic compartments of eukaryotic cells[93]. PGRN interacts with Sortilin on the cell surface through a high affinity binding mediated by the last 100 residues at the C-terminal of PGRN; a region that contains the granulin domain E and other C-terminal residues[92]. They described a process by which PGRN is expressed in activated microglia and, once secreted, it interacts in trans with Sortilin on motoneurons surface. PGRN is then internalized into the cell by endocytosis and directed to the lysosomes[93]. Through this mechanism, Sortilin is able to regulate extracellular PGRN levels and to maintain a correct neuronal function.

One year later, in 2011, Tang W. *et al.* demonstrated that PGRN is able to bind with high affinity the TNF receptor 1 (TNFR1) and the TNF receptor 2 (TNFR2). PGRN acts as a competitor of TNF-α on TNFRs inhibiting, in this way, the immune response[89]. This discovery supported the already known

PGRN anti-inflammatory function, and suggested the use of PGRN, or a synthetic PGRN fragment, as a therapeutic factor for diseases, like arthritis, characterized by a strong immune response[89].

2.3.5 GRN related diseases

In classical recessive disorders, heterozygous individuals are healthy carriers that do not show mutation-related symptoms. Classical dominant disorders are characterized by individuals that show the phenotype when the mutation occurs in heterozygous; usually homozygous are rare and the phenotype is a severe form of the heterozygous one. *GRN* mutations cause different clinicopathological phenotypes in heterozygous and homozygous forms[94]. *GRN* heterozygous null mutations are causative of Frontotemporal Dementia (FTD)[95], while homozygous mutations that produce a complete abolition of PGRN give rise to NCL11[94].

FTD is the second most common form of presenile dementia after Alzheimer disease. It represents 5-15% of all dementia and usually appears in people under 60 years of age[96,97]. FTD is an inherited autosomal dominant disease with incomplete penetrance[98,99]. It is characterized by neuronal atrophy of the frontal and anterior temporal lobes, which are involved in regulating behaviour, language and empathy. In fact the most evident symptoms are social withdrawal, apathy and behavioural changes[100]. Depletion of one *GRN* allele induce the formation, in neurons, of cytoplasmic and nuclear inclusions containing ubiquitinated and phosphorylated fragments of TAR DNA-binding protein 43 (TDP-43)[101,102]. TDP43 is an RNA-binding protein and splicing modulator that also binds *GRN* mRNA[103,104]. Loss of 50% of expressed or secreted PGRN is due to nonsense mutations or frameshift mutations that generate a Premature Termination Codon (PTC), with subsequent degradation of the transcript by the Nonsense-Mediated mRNA Decay (NMD)[105]. Other mutations can affect the signal peptide impairing PGRN secretion, or can modify a splicing donor thus leading to nuclear intron retention and transcript

degradation[106], as well as carry out the deletion of the whole copy of the *GRN* gene[107,108].

NCL11 is an inherited autosomal recessive disorder caused by homozygous null mutations in *GRN* gene[94]. As other NCLs, it is characterized by accumulation of lipofuscin, an aggregate of oxidized cross-linked proteins and lipids, into the lysosomes[109]. Smith *et al.* in 2012 described two cases of adult-onset NCL11 affecting siblings of Italian origins. The proband, a 28-year-old male, displayed progressive visual failure at 22 years followed by convulsions at 25 years and seizures at 26 years. He presented cerebellar ataxia, cerebellar atrophy, early cognitive deterioration and retinal dystrophy with optic nerve atrophy, vessel attenuation and irregular retinal pigmentation[94,110]. The proband's 26-year-old sister started having convulsions at 23 years and her vision began to deteriorate at 25 years old. She displayed cerebellar ataxia, cerebellar atrophy and retinal dystrophy[94,110]. Genetic analysis revealed a 4bp deletion in the *GRN* gene of the two siblings. The c.813_816delCATC (rs63749877) mutation generates a frameshift followed by a PTC[94]. The absence of PGRN was confirmed by analysis of circulating fluids and peripheral tissues. Skin biopsy revealed cytoplasmic vacuoles, empty or containing electrondense structures, and polymorphic lysosomal storage in glandular and endothelial cells[94,110].

Storage of abnormal autofluorescent lipopigments (lipofuscin) was impossible to check in human *GRN*$^{-/-}$ brain since patients are alive, but it was observed in the neurons of *Grn*$^{-/-}$ mice, which reproduce the NCL11 human pathology[111]. To date, five different mouse models of NCL11 (*Grn*$^{-/-}$) exist and all of them, which have different genetic backgrounds, show an accelerated accumulation of the aging pigment lipofuscin in the brains[72,112,113] suggesting a more rapid aging in neurons[115], associated with vacuolation in the habenula and hippocampus[114]. Lipofuscin accumulation occurs normally during aging and it is accounted as a cellular aging marker in post-mitotic cells like neurons. Its formation is due to mitochondrial repair mechanism defects, oxidative stress and dysfunction in the proteasomal and/or autophagic-lysosomal degradation systems[113,114]. These

observations support the already known PGRN function in neuronal survival[70] and a possible involvement of PGRN in the autophagic-lysosomal pathway.

2.4 Transcription Factor EB: the master regulator of autophagy and lysosomal biogenesis

Autophagy is a catabolic process by which the cytosolic material, including proteins, lipids and organelles, is directed to the lysosome and degraded[115-117]. Autophagy has an important role in regulating cellular quality control in neurons since the accumulating material cannot be reduced by cellular divisions[118], therefore autophagy impairment leads to neurodegenerative disease[118-120].

There are three types of autophagy: chaperone-mediated autophagy, microautophagy and macroautophagy. The Chaperone-mediated autophagy is based on the direct transport of the cytosolic proteins into the lysosome, in this case the proteins must be unfolded by chaperones. Microautophagy relies on the invagination of lysosomal membrane with subsequent import of a small amount of cytoplasmic material into the lysosome. Macroautophagy (referred to as autophagy) is the most studied and needs a double membrane organelle, the autophagosome, in order to deliver material to the lysosome[121] (Fig.3).

The autophagic process begins with the formation of a small vesicular sack called phagophore or isolation membrane. The phagophore elongates and incorporates a portion of cytoplasm leading to the formation of a double membrane structure called autophagosome. Afterwards, the outer membrane of the autophagosome fuses with the lysosome leading to the generation of the autolysosome. Inside the autolysosome all the material and the inner autophagosome membrane are degraded producing amino acids and other small molecules that will be delivered back to the cytosol for recycling or used to produce energy[121] (Fig.3).

Autophagosomes and lysosomes are the main actors of the so called “cell clearance process” by which the accumulated material is degraded and recycled. Settembre C. *et al*. demonstrated that biogenesis of autophagosomes and lysosomes is co-regulated by the transcription factor EB (TFEB)[122].

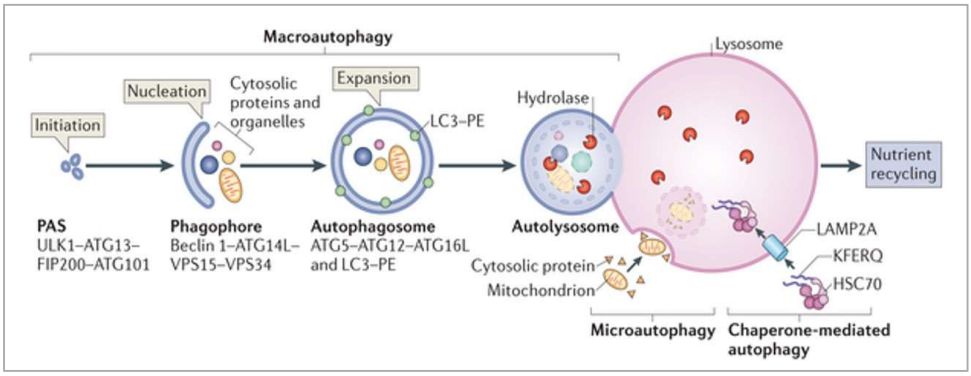

Fig.3 Image representing the three main autophagic processes: chaperon-mediated autophagy, microautophagy and macroautophagy. (Adapted from Kaur J. and Debnath J. 2015).

TFEB is a member of the microphthalmia-transcription factor E (MiT/TFE) subfamily of basic helix-loop-helix leucine zipper (bHLH-Zip) transcription factors[123]. It recognizes and binds a 10-base E-box-like palindromic sequence, the GTCACGTGAC motif, located within 200bp from the transcription start site and named Coordinated Lysosomal Expression and Regulation (CLEAR) element[124]. TFEB regulates the expression of genes related to lysosomal biogenesis and function[124] and activates the transcription of autophagic genes, all of which contain the CLEAR motif in their promoter[122].

TFEB activity is regulated by post-translational modifications. In basal conditions, under nutrient-rich conditions, TFEB is located into the cytoplasm with a particular enrichment on lysosomes. In starved condition (absence of nutrients) TFEB is located into the nucleus[122,124]. TFEB activation and localization depend on the activity of mammalian Target Of Rapamycin (mTOR), which is a kinase that localizes to the cytoplasmic surface of lysosomes as part of the mTOR Complex1 (mTORC1), and on the activity of Extracellular signal-Regulated Kinase 2 (ERK2), which belongs to the MAPK pathway[122,125-127]. mTORC1 is responsible for the phosphorylation of TFEB on Ser211[126,127], while ERK2 is responsible for the phosphorylation of Ser142[122]. In basal condition mTORC1 is active, localizes on lysosomal membrane, and phosphorylates TFEB recruiting it on lysosomes. Once phosphorylated, TFEB is in its inactive form, interacts with 14·3·3 protein and localizes into the

cytoplasm. In absence of nutrients, or in cases of lysosomal dysfunctions, mTORC1 is released from the lysosomal membrane and becomes inactive. TFEB, in its unphosphorylated and active form, moves to the nucleus where it activates the transcription of its target genes[126,127] (Fig.4).

As previously reported, LSDs are characterized by an accumulation of undegraded material in the lysosomal lumen due to genetic defects in specific lysosomal proteins[128,129]. LSDs mouse models show a significant nuclear localization of TFEB, indicating that the cellular response to the accumulation of undegraded material inside the lysosomes is based on the enhancement of lysosomal biogenesis[124]. In different publications it was demonstrated how the overexpression of TFEB, and so the induction of the autophagic-lysosomal pathway, in cellular and animal models of LSD, could ameliorate the phenotype leading to a reduction of the accumulated undegraded substrates in cells and tissues[130-133]. Therefore TFEB could be a suitable target of therapeutic strategies for LSDs and neurodegenerative disorders.

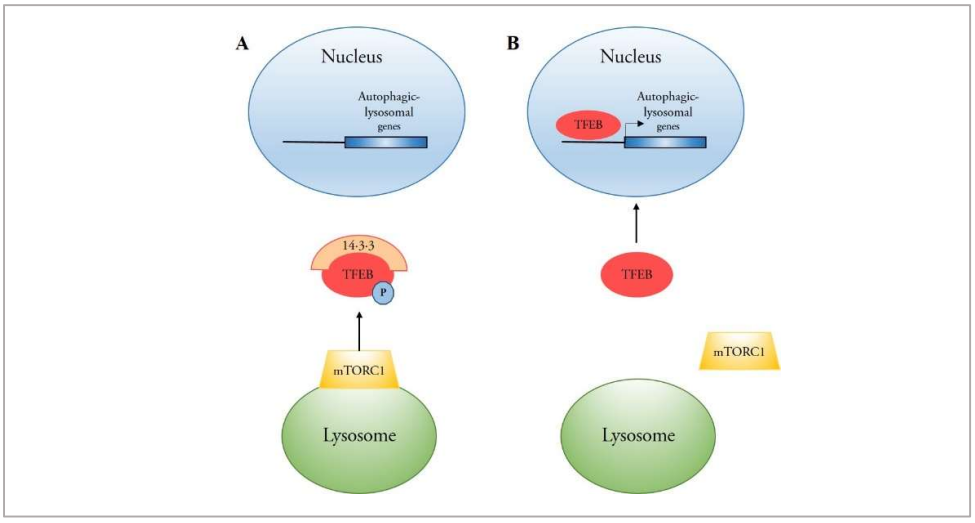

Fig.4 Representation of TFEB regulatory mechanism mediated by mTORC1. (A) Nutrient rich condition: active mTORC1 localizes to lysosomes and phosphorilates TFEB, which in turn interacts with the 14·3·3 protein and is retained into the cytosol. (B) Starvation: inactive mTORC1 is released from lysosomes and dephosphorylated TFEB migrates into the nucleus where it activates the autophagic and lysosomal target genes.

2.5 CRISPR-Cas9 system

Identification of gene function has always been the first step to develop successful therapies for genetic diseases. Reverse genetic and therefore, the generation of KO model systems, is actually the most powerful approach to unravel gene function.

In the recent years the most used genome editing technologies are based on the use of Zinc Finger Nucleases (ZFNs) and Transcription Activator-Like Effector Nucleases (TALENs). These are artificial fusion proteins composed by a DNA binding domain fused to a non specific nuclease domain which produces double strand breaks in a target genomic locus, with subsequent generation of mutations. In the last three years a new genome editing technology emerged: the Clustered Regularly Interspaced Short Palindromic Repeats (CRISPR)-Cas9 nuclease system.

CRISPR-Cas9 system is one of the protective systems that bacteria and archaea evolved as a defence mechanism against virus infections[134]. This adaptive immunity system is based on the ability of the CRISPR array to integrate fragments of exogenous DNA (spacers or protospacers), resulting in a sequence-specific resistance to the corresponding virus[135]. CRISPR-Cas mediated immunity occurs in three steps. The first one is the "acquisition stage", that is the integration of a new spacer into the CRISPR locus. The second step is the "expression stage" where the CRISPR array is transcribed and the precursor transcript is processed into smaller CRISPR RNAs (crRNAs). The last step is the "interference stage" characterized by the formation of Cas-crRNA complex which recognises and cleaves the invading DNA[136] (Fig.5).

Three different types of CRISPR-Cas systems exist. Type I systems are based on the Cas3 nuclease-helicase activity; type II systems are characterized by the activity of the Cas9 nuclease; type III systems are the less characterized, they involve the Cas10 which is a large protein whose function is unknown[136,137].

Type I and III CRSPR-Cas systems are present in archaea and bacteria while the CRISPR-Cas type II system is specific for bacteria.

CRISPR-Cas type II system from *Streptococcus pyogenes* is the well-known and best characterized. Type II system incorporates fragments of the invading DNA between the repeat sequences of the CRISPR array, the transcribed array is processed into crRNAs, which contain the protospacer sequence and part of the CRISPR repeat, then each crRNA hybridizes with a transactivating CRISPR RNA (tracrRNA)[138]. The crRNA-tracrRNA hybrid interacts with the Cas9 nuclease and drives it on the target DNA. The protospacer of the crRNA recognises the complementary sequence on the target DNA flanked by the Protospacer Adjacent Motif (PAM) and here the Cas9 generates a double-strand break followed by the degradation of the exogenous DNA[139,140] (Fig.6A).

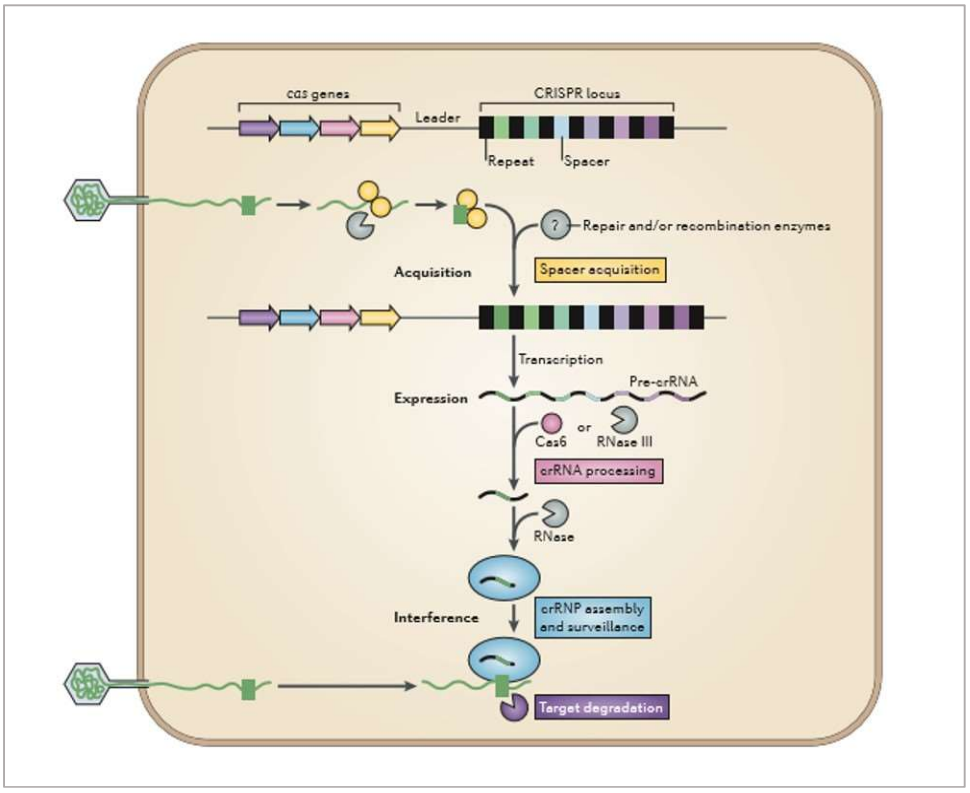

Fig.5 Adaptive immunity CRISPR–Cas system: acquisition (yellow), crRNA processing (pink), crRNA assembly and surveillance (blue) and target degradation (purple). The acquisition stage is characterized by the entry and fragmentation of the invading DNA, so that a new protospacer

(green) is integrated into the CRISPR array. During the expression stage the CRISPR locus is transcribed and the pre-crRNA is processed, by CRISPR-associated (Cas6) and/or housekeeping ribonucleases (such as RNase III), into small crRNAs. The Cas proteins and mature crRNAs are assembled into a crRNP complex in the interference stage, during which the crRNA recognizes the target DNA and induces the Cas mediated cleavage, followed by the target degradation. (John van der Oost, *et al.* 2014).

This type II system of *S. pyogenes* has been adapted to achieve genome editing in cellular and animal models. The crRNA and the tracrRNA were fused to generate a chimeric single-guide RNA (gRNA)[141] containing, at the 5', 20 nucleotides (corresponding to the protospacer crRNA sequence) which recognise the target DNA sequence followed by the PAM 5'-NGG sequence[142,143] (Fig. 6B and 7). Once introduced, or expressed, the Cas9 and the gRNA into the model system, the gRNA interacts by Watson and Crick base pairing with the target site driving the Cas9 at the desired locus. The Cas9 introduces, ~3 bp upstream the PAM sequence, a double strand break (DSB) which typically undergoes one of two major pathways for DNA damage repair: the error-prone Non-Homologous End Joining (NHEJ) or the high-fidelity Homology Directed Repair (HDR) pathway[142,144] (Fig.8). In the NHEJ pathway the ends of the DSB are re-joined with insertions or deletions of some nucleotides (INDEL mutations) which, in the coding sequence, can result in frameshifts and subsequent generation of PTCs leading to gene KO. The HDR pathway can be used to introduce specific mutations. This mechanism needs a DNA repair template (called "donor DNA") in form of plasmid or single-stranded DNA oligonucleotides (ssODNs). HDR pathway is triggered less frequently than NHEJ and occurs only in dividing cells. Moreover, HDR efficiency depends on several factors such as the genomic locus, the repair template and the cell type and state[144].

CRISPR-Cas9 technology is the most powerful system for genome editing and offers the possibility to target different genomic loci simultaneously. In fact, the Cas9 can be re-targeted to a new genomic site only changing the 20nt gRNA sequence and Cas9 domains (HNH and RuvC) can be mutated in order to

generate different forms of Cas9 nucleases, therefore expanding the range of CRISPR-Cas9 technology applications[145].

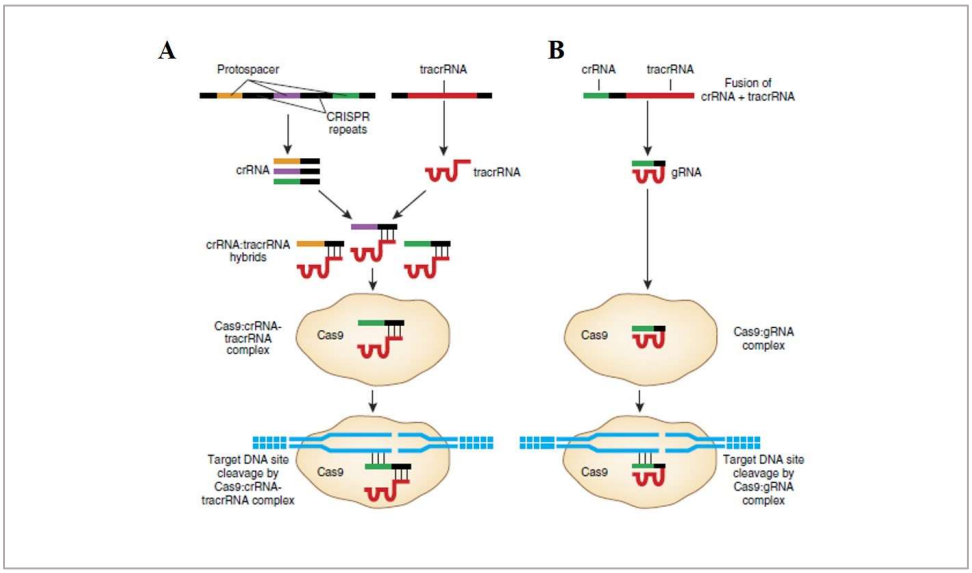

Fig.6 Naturally occurring and engineered CRISPR-Cas systems. (A) CRISPR system type II of *S.pyogenes*: the exogenous DNA is integrated into the CRISPR array; the crRNAs, containing the protospacer region, hybridize to tracrRNAs encoded by the CRISPR system; the crRNA-tracrRNA hybrid associates with the Cas9 forming a complex that recognizes and cleaves the invading DNA bearing the protospacer sequence. (B) The engineered CRISPR-Cas9 system is based on the fusion of crRNA and a portion of tra-crRNA sequences. This single gRNA forms a complex with the Cas9 that induces the cleavage of the target DNA sequence complementary to the 5' 20 nucleotides of the gRNA. (Sander J.D., *et al.* 2014)

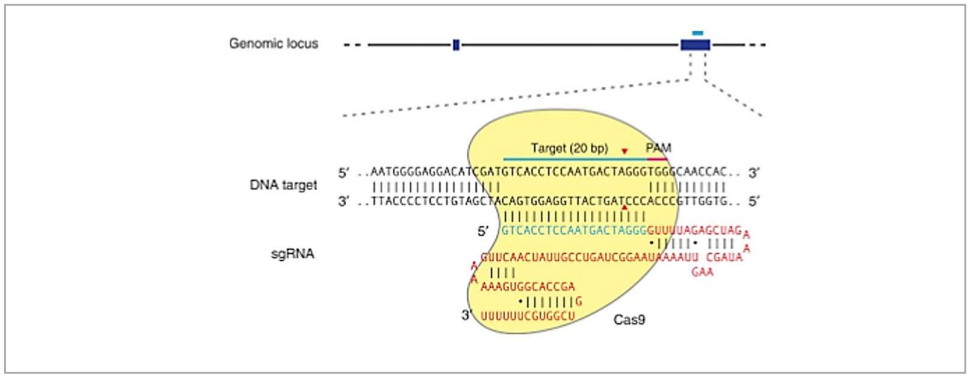

Fig.7 *Sp*Cas9 interacting with gRNA. Cas9 nuclease from *S. pyogenes* (yellow) is recruited on the target site by a gRNA consisting of a 20-nt guide sequence (blue) and a scaffold (red). The

guide sequence pairs with the DNA target (blue bar on top strand), directly upstream the 5′-NGG adjacent motif (PAM; pink). Cas9 mediates a DSB ~3 bp upstream the PAM sequence (red triangle). (Ran F.A., *et al*. 2013)

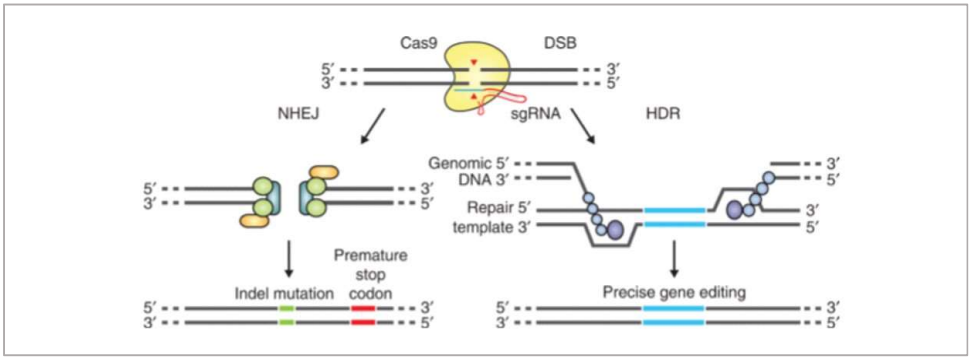

Fig.8 DNA damage repair mechanisms: Non-Homologous End Joining (NHEJ) and Homology Directed Repair (HDR). The NHEJ pathway induces the insertion or deletion of nucleotides (INDEL mutations) which can lead to frameshifts and generation of a PTC. The HDR pathway allows a precise genome editing in presence of a DNA template carrying single nucleotide substitution or a specific sequence that must be inserted into the genomic target site. (Ran F.A., *et al*. 2013)

To date, different Cas9 mutants have been generated. Cas9 RuvC1 catalytic domain was mutated with an aspartate-to-alanine substitution (D10A) to produce a Cas9 nickase mutant (Cas9n). Cas9n generates single strand DNA cleavages, instead of DSB, in the target sites, therefore promoting the HDR rather than the NHEJ DNA repair mechanism[144]. A double Cas9 mutant, which contains two mutations into the RuvC1 and HNH nuclease domains (D10A and H841A), was generated and it was demonstrated that this "dead" Cas9, which lost its cleavage activity, can be used to knock down gene expression in mammalian cells[146].

Despite the CRISPR-Cas9 system offers lots of advantages with respect to other genome editing tools, the main problem of this approach is the off-targets cleavage. Lots of bioinformatic programs, which allow the recognition of off-target sites by gRNAs, raised up recently and many studies were conducted to overcome this limit. Since it was demonstrated that the CRISPR-Cas9 is sensitive to mismatches close to the PAM sequence, as two or more mismatches

in this region completely abolished the CRISPR-Cas9 nuclease activity[145,147,148], a possible strategy to avoid off-target cleavages involves the design of gRNAs that present three or more mismatches at the 3' of the gRNA sequence[149]. A different strategy, aimed to reduce the off-targets cleavage, was developed in 2016 by Slaymaker I.M. *et al.* They generated some Cas9 mutants carrying alanine substitutions in the groove between the HNH, RuvC and PAM interacting domains. This positively charged groove interacts and stabilizes the non-target DNA strand of the target DNA. Abolition of positive charges enhances the rehybridization between the target and non target DNA strands, so a more stringent Watson and Crick base pairing is necessary between the target DNA strand and the gRNA[150].

3. Aim of the work

Because of the storage of lipofuscin inside to the lysosomes, NCL11 is a genetic disease classified as LSD. The molecular mechanisms leading to the pathogenesis of NCL11 is still poorly understood and very few is known about the function of *GRN*, the gene that, if mutated, is causative of this disease. The absence of a good therapy for NCL11 patients is a consequence of this lack of knowledge. Indeed, available therapies for the treatment of these patients are only aimed to ameliorate their pathological status without stopping the degeneration associated with the disease. The goal of this project was to generate a good cellular model system with low degree of variability and, therefore, suitable for cell biology and HCS experiments that actually are not feasible with the available tools. By the use of this cellular model, I performed experiments aimed to unravel the cellular role of *GRN* within lysosomes and to find new suitable therapies for the treatment of NCL11 patients. For the generation of this cellular model I took advantage of the CRISPR-Cas9 technology in order to knock out the *GNR* gene in Arpe19 (retinal pigmented epithelium) cells. *GRN* edited cell lines were characterized in order to define the NCL11 phenotype. The autophagic-lysosomal pathway was investigated in *GRN* KO cells in order to highlight the impaired mechanisms that are responsible for lipofuscin accumulation. The underlined phenotype was then analysed by OPERA system, through a specific script, in order to quantify the lysosomal defects in *GRN* KO cells. All these results will be used to perform a High Content Drugs Screening aimed to find new suitable therapies for the treatment of NCL11 affected patients.

4. Materials and Methods

4.1 Cell culture, transfections and plasmids

Arpe19 were purchased from ATCC and cultured in DMEM-F12 (Invitrogen) supplemented with 10% FBS, 1% penicillin/streptomycin and 2mM L-Glutamine (Euroclone). Cells were grown at 5% CO_2 at 37°C. Starvation treatments were performed in HBSS-10mM Hepes. Cells were rinsed twice with starvation medium, then kept in a full volume of starvation medium for 1h. Bafilomycin A1 (100nM) (Sigma Aldrich) was added in the culture medium and cells were treated for 1h.

Plasmids preparation was performed with CompactPrep Plasmid Maxi Kit (QIAGEN). Arpe19 cells were transfected with Amaxa® Cell Line Nucleofector® Kit V for all-in-one vector (pGS-CMV-Cas9/PURO, GeneCopoeia) containing the gRNA sequence and with Lipofectamine 2000 (Invitrogen) for LC3-RFP–GFP plasmid (from T. Yoshimori) following the manufacturer's protocol.

4.2 Generation of $GRN^{+/-}$ and $GRN^{-/-}$ clones

To obtain *$GRN^{+/-}$* and *$GRN^{-/-}$* Arpe19 clones, $1x10^6$ cells were nucleofected with the all-in-one vector (pGS-CMV-Cas9/PURO, GeneCopoeia) containing the gRNA sequence. 24h after nucleofection, 0.2 µg/ml puromycin was added to cell culture for one week. The transfected cell pool was plated into 96-well plate by single cell sorting using DB FACSAria. Sorted cells were kept in culture until confluence, then the 96-well plate was duplicated, one aimed to cell growth and the other one aimed to DNA extraction. For genomic DNA extraction cell clones were washed twice with PBS and 60ul of DirectPCR Lysis Reagent (Viagen) was added to the plate following the manufacturer's protocol. 2ul of genomic DNA preparation was used to perform the PCR in order to amplify the genomic locus of interest. AmpliTaq Gold® 360 Master

Mix (Thermo Fisher Scientific) and two primers (Forward: 5'-CACCAGCTCCTTGTGTGATG-3' and reverse: 5'-CTGTTAGTCCTCTGGGCAGG-3') were used for PCR amplification following the manufacturer's protocol. PCR products were subjected to Sanger sequencing in order to identify INDEL mutations.

4.3 Western blotting

$1{,}5x10^5$ cells were plated in 6-well plates. 48h after plating, cells were washed twice with PBS and then scraped in RIPA lysis buffer (20 mM Tris pH 8.0, 150 mM NaCl, 0.1% SDS, 1% NP-40, 0.5% sodium deoxycholate) in the presence of PhosSTOP tablets (Roche) and Protease Inhibitor Cocktail (Sigma). Cell lysates were incubated on a shaker for 30 min at 4°C. Samples were then put 3 min in dry-ice and 3 min in a 37°C water bath (repeated for three times). The soluble fraction was isolated by centrifugation at 13,000 r.p.m. for 20 min at 4 °C. Protein concentration was measured by using colorimetric Bradford method (Bio-rad). Samples were mixed with Laemmli buffer containing β-mercaptoethanol, boiled 80°C for 10 min and resolved by SDS-PAGE. Electrophoresis was run at 100V constant in MOPS buffer (2.5mM MOPS, 2.5mM Tris Base, 0.1% SDS, 1mM EDTA, pH 7.7). Proteins were blotted onto polyvinylidene fluoride (PVDF) membranes and blocked for 1 hour with non-fat 5% milk diluted in PBS-0,1%Tween 20 (PBS-T). Membranes were probed with primary antibodies, diluted with BSA 5% in PBS-T, overnight at 4°C. The next day membranes were washed twice in PBS-T and incubated with corresponding HRP-labelled secondary antibodies (Calbiochem) in 2.5% milk in PBS-T. After three washes in PBS-T, protein visualisation was performed using the Super Signal West Dura substrate (Thermo Scientific). The western blotting images were acquired using the Chemidoc-lt imaging system (UVP) and band intensity was calculated using ImageJ software using the 'Gels and Plot lanes' plug-in. Antibodies used for western blotting are: β-actin (Sigma, cat. A5316, 1:10000), PCDGF (PGRN) (Invitrogen, cat. 40-3400, 1:500), LAMP-1 (Santa Cruz, cat. sc-20011, 1:1000), LC3 (Novus, cat. NB100-2220,

1:2000), TFEB (Cell Signalling, cat. 4240, 1:1000), 4EBP1 (Cell Signalling, cat. 9644, 1:1000), phospho-4EBP1 (Ser65) (Cell Signalling, cat. 9456, 1:1000).

4.4 Quantitative real-time PCR

Wt, *GRN*$^{+/-}$ and *GRN*$^{-/-}$ Arpe19 cells were plated into 6-well plates ($1.5x10^5$ cells/well). RNA extraction was performed after 48h by RNeasy Mini Kit (Qiagen). 500ng of each RNA sample was reverse transcribed to single-stranded cDNA by using QuantiTect Rev Transcription Kit (Qiagen) in a final reaction volume of 20µl. cDNA mixes were diluted 1:6 in water, and 3µl of the diluted cDNA solution was analysed by Real-Time PCR. Real-time PCR was performed using LightCycler® 480 SYBR Green I Master (Roche) and performing the reaction in the LightCycler® 96 System (Roche). The parameters of Real-time PCR amplification were defined according to Roche recommendations. To quantify gene expression, beta-2-microglobulin (B2M) mRNA expression was used as an internal reference. Primers used in this work:

B2M forward: GCTCGCGCTACTCTCTCTTT

B2M reverse: CAATGTCGGATGGATGAAACCC

GRN forward: CCAGATGCCTGCTCAGTGT

GRN reverse: AGATGGTCAGTTCTGCCCTG

TFEB forward: CAAGGCCAATGACCTGGAC

TFEB reverse: AGCTCCCTGGACTTTTGCAG

MCOLN1 forward: GAGTGGGTGCGACAAGTTTC

MCOLN1 reverse: TGTTCTCTTCCCGGAATGTC

WIPI forward: GCACAATCTCCCCTGAAGTC

WIPI reverse: CCTCCTGGATATTCCTGCAA

ATP6V0E1 forward: CATTGTGATGAGCGTGTTC

ATP6V0E1 reverse: AACTCCCCGGTTAGGACCCTTA

4.5 Cell immunofluorescence

$1x10^5$ Arpe19 cells were plated in 8-well Lab-Tek Chamber Slide (Nunc) or in Cell Carrier™-96 plate (Perkin Elmer) for HCS analysis. 48h after plating, cells were fixed for 10 min in 4% PFA in PBS and then washed with PBS. For the detection of endogenous LC3, cells were fixed with cold methanol. Permeabilization and blocking was performed with 3% BSA-0.02% saponin in PBS (Blocking solution) for 1h. Cells were incubated with primary antibodies, diluted in blocking solution, over night at 4°C. The day after, cells were washed three times for 10 min with blocking solution and incubated for 1h with the secondary antibody (AlexaFluor-labelled) diluted 1:200 in blocking solution. For Shiga toxin staining, cells were incubated with 140 ng/ml Shiga (from J. Ludger) in blocking solution, together with secondary antibody, for 1h. After three washes of 10 min with blocking solution, slides were mounted with Vectashield mounting medium with dapi (Vector Laboratories) or, cells plated in 96-well-opera plates were incubated with DAPI for 5 min. Primary antibodies used for immunofluorescence experiments are: LAMP-1 (Santa Cruz, cat. sc-20011, 1:400), LC3 (Novus, cat. NB100-2220, 1:100). Shiga toxin-LAMP1 co-staining was detected by Zeiss LSM 880 Airyscan. Other confocal acquisitions were performed by Zeiss LSM 800.

4.6 LysoTracker assay

$1x10^6$ Arpe19 cells were collected and centrifuged at 1200 rpm for 5 min. Cell pellet was resuspended in 1ml PBS and incubated 5 min with LysoTracker Red DND-99 (Invitrogen) diluted 1:1000. After two washes in PBS, followed by centrifugation as previously described, cells were resuspended in FACS solution (0.5% Trypsin – 5mM EDTA- 1% FBS in PBS) and fluorescence was analysed by Fluorescence-Activated Cell Sorting (FACS) using DB FACSAria.

4.7 High Content Screening and Electron Microscopy

High Content Screening analysis were performed by D. Medina's HCS facility at TIGEM. Opera system was used to acquire 15 fields for each sample at 40x magnification. Analysis of each field was performed by Columbus software (PerkinElmer) using the parameters listed in table 1. Electron Microscopy was performed by E. Polishchuk (Advanced Microscopy and Imaging facility, TIGEM).

Table 1. *Columbus analysis parameters*

Select Population (2)	**Population :** Nuclei	**Method :** Common Filters Remove Border Objects Region : Cell	Output Population : Nuclei Selected
Find Nuclei	**Channel :** Exp1Cam1 **ROI :** None	**Method :** B Common Threshold : 0.2 Area : > 90 µm² Split Factor : 7 Individual Threshold : 0.4 Contrast : > 0.1	Output Population : Nuclei
Find Cytoplasm	**Channel :** Exp3Cam2 **Nuclei :** Nuclei	**Method :** D Individual Threshold : 0.05	
Find Spots	**Channel :** Exp3Cam2 **ROI :** Nuclei Selected	**Method :** B Detection Sensitivity : 0.45 Splitting Coefficient : 1 Calculate Spot Properties	Output Population : TOTAL SPOT
Calculate Morphology Properties	**Population :** TOTAL SPOT **Region :** Spot	**Method :** Standard Area Roundness	Output Properties : Spot

4.8 Statistics

GraphPad Prism (GraphPad Software, San Diego, CA) was used for all the statistical analysis. Statistical analyses of data were performed using Welch's t-test. Unpaired t-test was applied to two independent groups, e.g. wt versus KO. This test compares the means of the two groups of data to determine whether the data have come from the same population or not. A p-value was calculated, where p is the probability of a false positive event. P-value <0.05 indicates that the false-positive rate is very low and was considered significant.

5. Results

5.1 Generation of GRN KO Arpe19 cell line by CRISPR-Cas9 system

5.1.1 In silico strategy design

Bioinformatic analysis were performed in order to design two gRNAs targeting the coding sequence of *GRN* gene. The human *GRN* sequence is available on NCBI, Genbank NC_000017.11 (https://www.ncbi.nlm.nih.gov/nuccore/NC_000017.11?report=genbank&_from=44345086&to=44353106). The first step to identify suitable gRNAs was to check the presence of repetitive elements in the target region, in order to reduce the risk of off-target events. The exon 5 of *GRN* was scanned using the RepeatMasker software available on line (http://www.repeatmasker.org/cgi-bin/WEBRepeatMasker). Results reported in Fig.9 show that there are not repetitive elements in the input sequence.

Fig.9 RepeatMasker output: the software scanned the input sequence (*GRN* exon 5) for repetitive elements. Output analysis shows that there are not repetitive elements in the selected sequence.

ZiFiT Targeter software was used to identify possible gRNAs in the *GRN* exon 5 sequence (http://zifit.partners.org/ZiFiT/CSquare9Nuclease.aspx). With this program, it is possible to scan the input sequence for PAM motifs (NGG). The chosen setting parameters were: human genome and 20 nt as length of target site. The ZiFiT Targeter software allows the identification of off-targets indicating the numbers of mismatches for each off-target site. Two gRNAs were identified: the gRNA1 (CGAACTGACTATCAGGGCACCGG) recognizes three off-target sites, each of them with three mismatches, so reducing the risk of unwanted cleavages; the gRNA2 (ACGTGCTGTGTTATGGTCGATGG) does not recognize off-target sites (Fig.10).

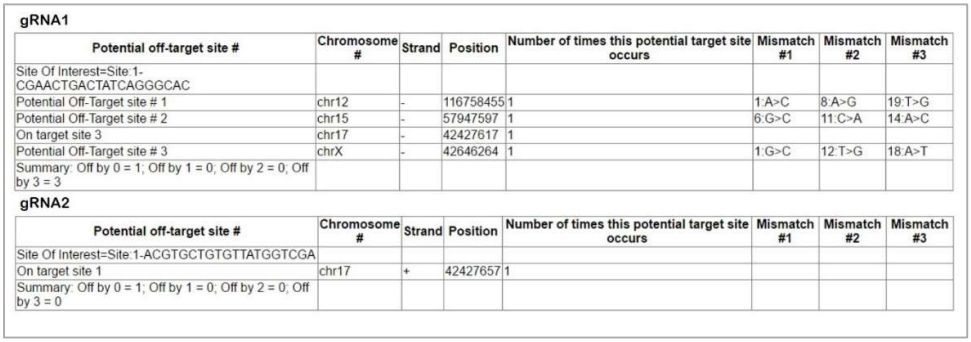

gRNA1

Potential off-target site #	Chromosome #	Strand	Position	Number of times this potential target site occurs	Mismatch #1	Mismatch #2	Mismatch #3
Site Of Interest=Site:1-CGAACTGACTATCAGGGCAC							
Potential Off-Target site # 1	chr12	-	116758455	1	1:A>C	8:A>G	19:T>G
Potential Off-Target site # 2	chr15	-	57947597	1	6:G>C	11:C>A	14:A>C
On target site 3	chr17	-	42427617	1			
Potential Off-Target site # 3	chrX	-	42646264	1	1:G>C	12:T>G	18:A>T
Summary: Off by 0 = 1; Off by 1 = 0; Off by 2 = 0; Off by 3 = 3							

gRNA2

Potential off-target site #	Chromosome #	Strand	Position	Number of times this potential target site occurs	Mismatch #1	Mismatch #2	Mismatch #3
Site Of Interest=Site:1-ACGTGCTGTGTTATGGTCGA							
On target site 1	chr17	+	42427657	1			
Summary: Off by 0 = 1; Off by 1 = 0; Off by 2 = 0; Off by 3 = 0							

Fig.10 gRNAs design and identification of off-target sites by ZiFiT Targeter software. Two gRNAs targeting the exon 5 of *GRN* were selected. The first gRNA (gRNA1) anneals with the plus strand of the target locus and is able to recognize three different off-target sites. The second gRNA (gRNA2) anneals with the minus strand and does not recognize off-target sites.

5.1.2 In vivo application of CRISPR-Cas9 genome editing technology

"All in one" strategy was chosen to efficiently achieve the genome editing of *GRN*. With this strategy it is possible to obtain one plasmid carrying both the human codon optimized wt Cas9 coding sequence, under the CMV promoter, and the gRNA sequence downstream the U6 promoter. gRNA sequence was cloned by Genecopoeia company into the pGS-CMV-Cas9/PURO vector containing puromycin resistence (Fig.11).

Arpe19 (retinal pigmented epithelium) cells were nucleofected with the vector carrying the Cas9 and the two gRNAs separately. After one week of selection with antibiotic, transfected cells were plated into 96 well plate in order to obtain single-cell derived colonies carrying the INDEL mutations. Single cell clones were duplicated into two different 96 well plates: one aimed to cell growth, the second one aimed to genomic DNA extraction, PCR amplification of the target locus and DNA Sanger sequencing in order to detect the INDEL mutations (Fig.11). Through Sanger sequencing only wt clones were detected using gRNA1, indicating that this guide was unable to drive the Cas9 to the target genomic site. By contrast, 50% of mutations were obtained with the gRNA2, 30% of which carrying heterozygous mutations and 20% homozygous mutations (Fig.12A). Two *GRN* mutated clones were selected and characterized.

The heterozygous clone sequencing displays a double peak starting from the Cas9 cleavage site. The homozygous clone presents 1bp (T/A) insertion in the gRNA target sequence, which generates a translational frameshift and a PTC, giving rise to a truncated PGRN protein, made of the half-granulin P and granulin G (Fig.12B).

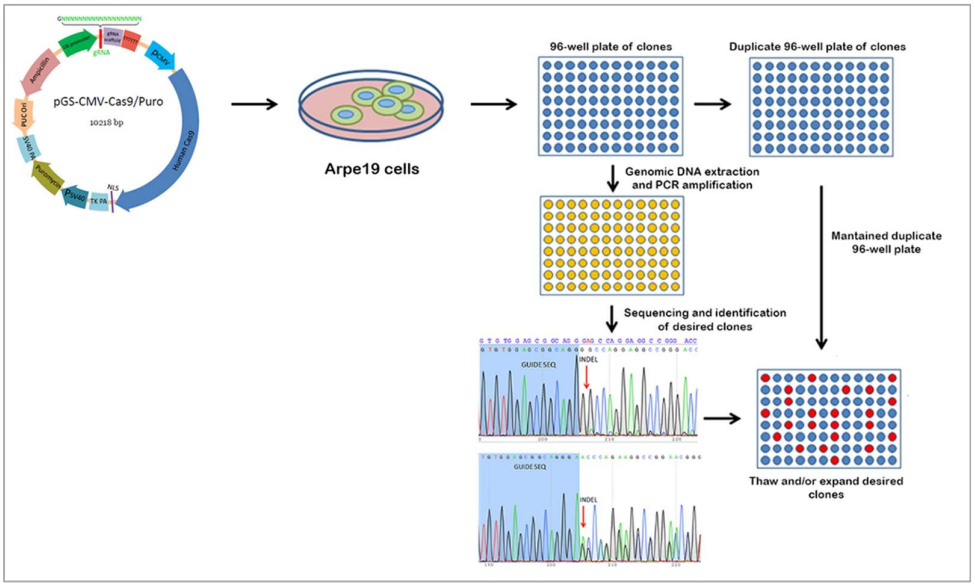

Fig.11 CRISPR-Cas9 working flow chart: Arpe19 cells were transfected with the "all-in-one" vector containing the two gRNAs separately. Transfected cells were selected with puromycin and plated, by single cell sorting, into 96 well plate. The 96well plate of clones was duplicated to cell growth and to genomic DNA extraction, PCR amplification and sequencing. Cell clones carrying INDEL mutations were selected.

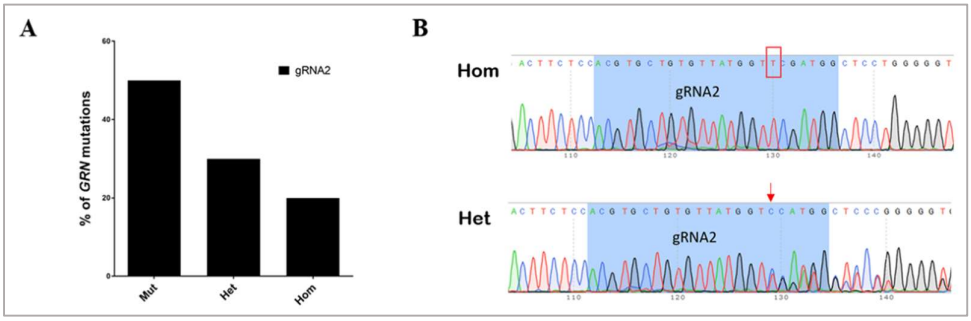

Fig.12 CRISPR-Cas9 strategy results. (A) Percentage of Cas9 efficiency. Cas9 cleavage efficiency was 0% for gRNA1 and 50% for gRNA2. Among all the INDEL mutations (Mut) in the target site 2, 30% were heterozygous (Het) and 20% homozygous (Hom). (B) Electropherograms of two *GRN* mutated clones: the homozygous clone shows a T insertion (red rectangle) 3bp upstream the PAM sequence; the heterozygous clone presents a double peak electropherogram starting from 3bp upstream the PAM sequence (red arrow). gRNA2 sequence is highlighted with blue.

5.2 Validation of $GRN^{+/-}$ and $GRN^{-/-}$ Arpe19 cell lines

$GRN^{+/-}$ and $GRN^{-/-}$ Arpe19 clones were validated by Real Time qPCR and Western blot (WB) analysis to detect *GRN* mRNA levels and PGRN protein expression levels. I revealed that PGRN protein expression is null in $GRN^{-/-}$ clone and half in $GRN^{+/-}$ clone compared to wt cells. As well as the real time analysis indicates that in $GRN^{+/-}$ clone *GRN* mRNA levels are half when compared to the wt, while in $GRN^{-/-}$ clone there is a four-fold reduction of the *GRN* mRNA amount (Fig.13A-B).

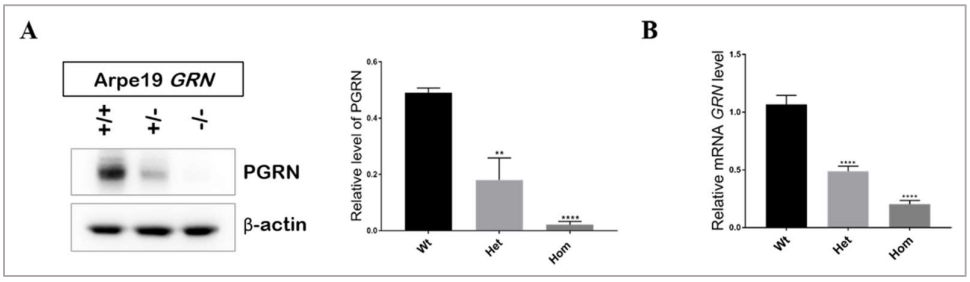

Fig.13 Validation of $GRN^{+/-}$ and $GRN^{-/-}$ clones. (A) Western blot was performed to detect the PGRN levels in wild type (Wt), heterozygous (Het) and homozygous (Hom) cell lines. Results confirm a reduction in PGRN levels in $GRN^{+/-}$ and $GRN^{-/-}$ clones. Graph shows densitometry analysis of the Western blot bands. Values are normalized to actin and are shown as an average (** $P \leq 0.01$, **** $P \leq 0.0001$, Welch's t-test). (B) *GRN* transcriptional levels in Arpe19 $GRN^{+/+}$, $GRN^{+/-}$ and $GRN^{-/-}$ clones. Values are shown as an average (**** $P \leq 0.0001$, Welch's t-test).

5.3 Shiga toxin accumulation assay

Storage of undigested material inside the lysosomes, in $GRN^{+/-}$ and $GRN^{-/-}$ cells, was checked using Shiga toxin accumulation assay. Shiga toxin is a toxin derived from *Shigella dysenteriae 1* that interacts with Globotriaosylsphingosine (Gb3), a glycosphingolipid whose accumulation was demonstrated in other LSDs[151]. Immunofluorescence experiments were performed in order to follow Shiga toxin accumulation together with an antibody against the lysosomal marker Lysosomal-Associated Membrane Protein 1 (LAMP1). Co-staining of the red-fluorescent Shiga toxin and the

lysosomal marker LAMP1, displays a specific lysosomal storage of undegraded material only in *GRN*$^{-/-}$ cells (Fig.14).

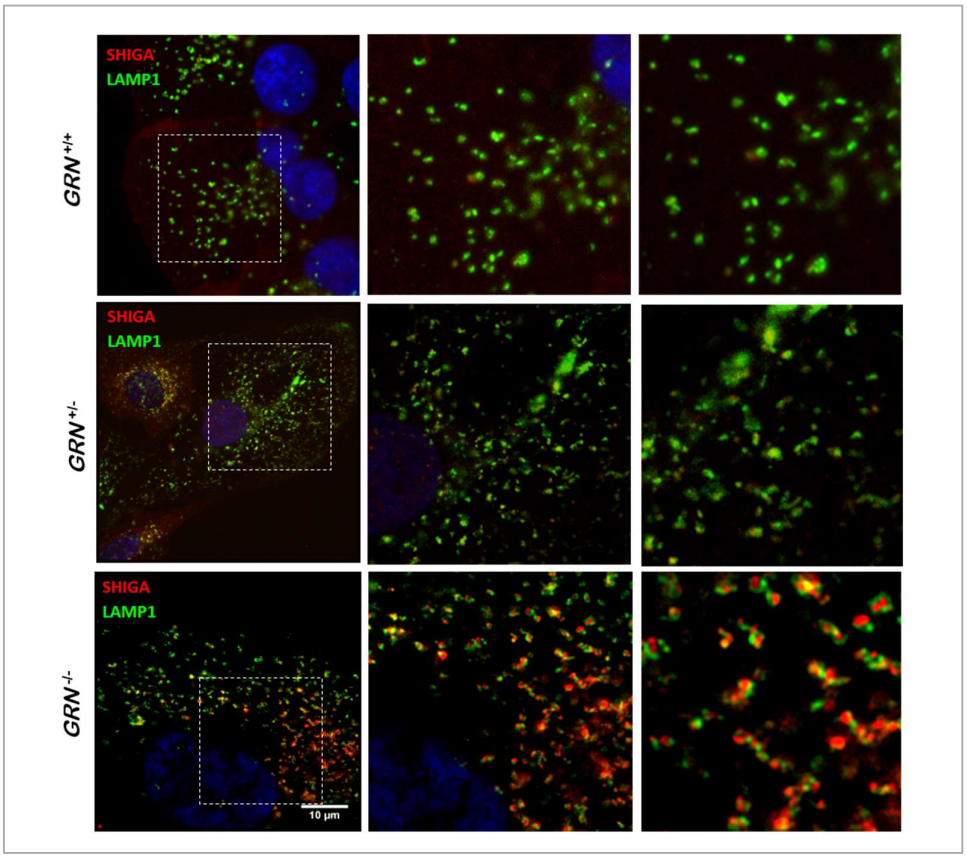

Fig.14 Gb3 accumulation in *GRN*$^{+/+}$, *GRN*$^{+/-}$ and *GRN*$^{-/-}$ Arpe19 cells. Co-staining of Shiga toxin (red) and the lysosomal marker LAMP1 (green) shows a lipid accumulation, inside the lysosome, in *GRN*$^{-/-}$ cells.

5.4 Analysis of lysosomal phenotype

The amount of lysosomes in *GRN*$^{+/-}$ and *GRN*$^{-/-}$ Arpe19 cell lines was assayed by WB experiment using the antibody against LAMP1. These experiments revealed that in *GRN*$^{-/-}$ cells the amount of LAMP1 protein was considerably increased, while in *GRN*$^{+/-}$ cells, LAMP1 amount was comparable to wt cells (Fig.15A). Detection of lysosomes was also assayed by FACS experiments using the LysoTracker series of probes, which are weak bases attached to fluorophores. Weak bases are unprotonated at physiological pH so that they can

permeate cells and their organelles. Upon protonation in acidic environment, such as the lysosome, they become "trapped"[152]. FACS analysis was performed in both *GRN*$^{-/-}$ and *GRN*$^{+/-}$ cells and obtained data confirmed that in *GRN*$^{+/-}$ cell line the amount of lysosomes is normal, while in *GRN*$^{-/-}$ cells there is a considerable increase represented by the pick shift between wt and KO cells (Fig.15B).

More important, LAMP1 immunostaining was also analyzed by HCS quantization. To this end, an *"ad-hoc"* script was designed to perform lysosomal morphometric analysis in the *GRN*$^{-/-}$ and *GRN*$^{+/-}$ Arpe19 cell lines. These results also confirmed the increased amount of lysosomes in absence of PGRN and revealed a lysosomal aggregation phenotype in the perinuclear region in *GRN*$^{+/-}$ but not in *GRN*$^{-/-}$ cells (Fig.16A-B).

Lysosomal morphology was validated by Electron Microscopy (EM) experiments. Obtained EM images display bigger lysosomes in *GRN*$^{-/-}$ cells than in the wt ones (Fig.17A). Furthermore, in absence of PGRN, I observed a different lysosomal distribution. Indeed, in *GRN*$^{-/-}$ lysosomes are located closer to the plasma membrane than the lysosomes observed in wt cells (Fig.17B).

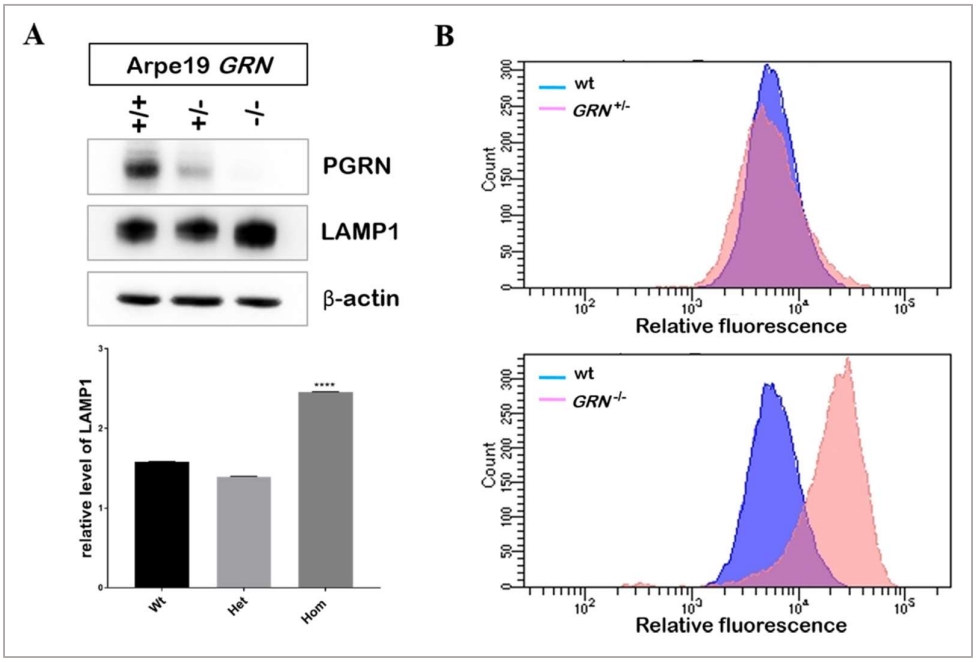

Fig.15 Detection of lysosomes amount. (A) Western blot showing LAMP1 protein levels in *GRN*$^{+/-}$ and *GRN*$^{-/-}$ cell lines. Wild type (Wt), heterozygous (Het), homozygous (Hom). Graph shows densitometry analysis of the Western blot bands. Values are normalized to actin and are shown as an average (**** P ≤ 0.0001, Welch's t-test). (B) FACS mediated detection of LysoTracker probes fluorescence. Pick shift between wt and *GRN* KO cells represents the increased amount of lysosomes.

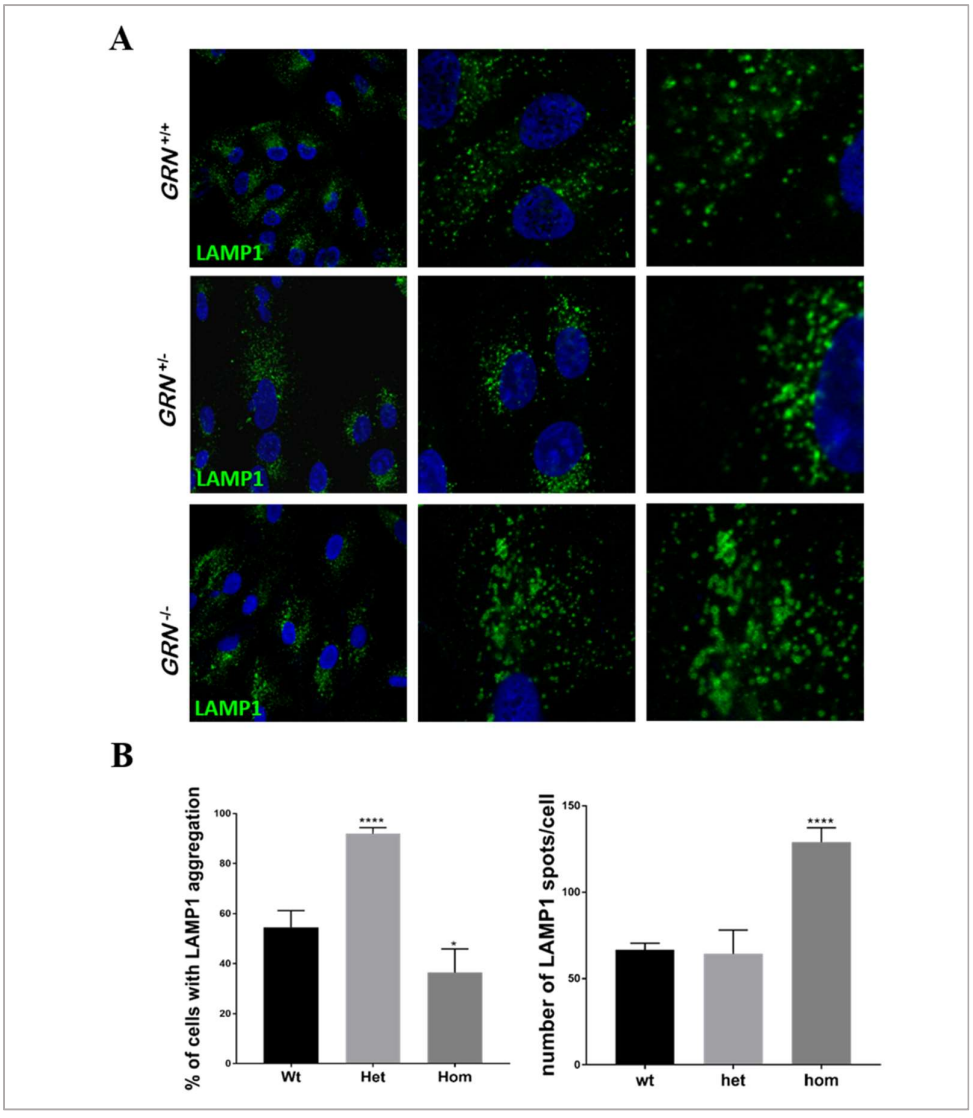

Fig.16 Lysosomes amount and aggregation. (A) LAMP1 immunostaining (green) reveals an increased number of lysosomes in *GRN*$^{-/-}$ cells and a perinuclear distribution of lysosomes in *GRN*$^{+/-}$ cells. (B) HCS analysis confirms the higher number of lysosomes per cell in absence of PGRN (upper graph) and evinces an aggregation of lysosomes in heterozygous condition (lower

graph). Wild type (Wt), heterozygous (Het), homozygous (Hom). Upper graph reports the number of LAMP1 spots per cell, lower graph shows the percentage of cells with LAMP1 aggregation. Values are shown as an average (* $P \leq 0.05$, **** $P \leq 0.0001$, Welch's t-test).

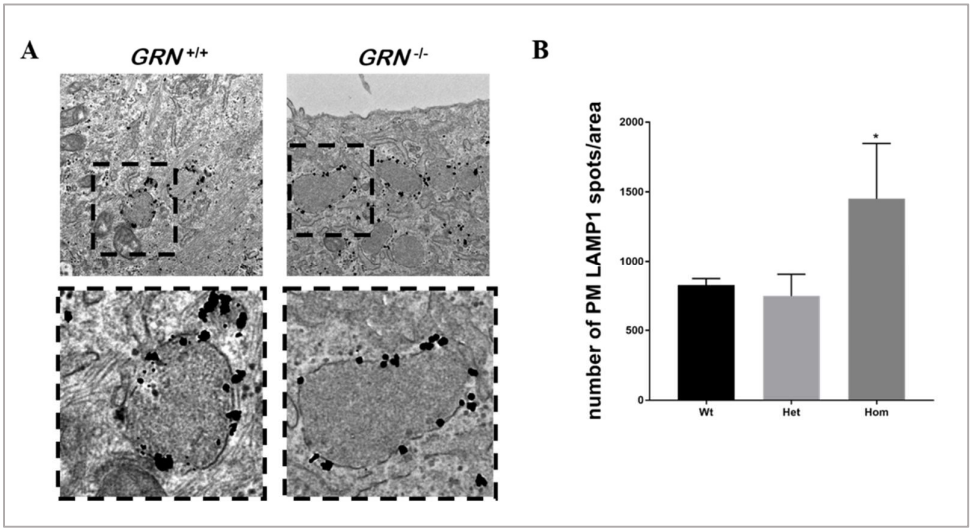

Fig.17 Lysosomal morphology and positioning. (A) Electron microscopy images of *GRN*$^{+/+}$ and *GRN*$^{-/-}$ cells. *GRN*$^{-/-}$ cells show bigger lysosomes with respect to cells with normal PGRN levels. (B) HCS analysis showing an increased number of lysosomes located to the plasma membrane (PM) in absence of PGRN. Wild type (Wt), heterozygous (Het), homozygous (Hom). Values are normalized to the number of LAMP1 spots per area and are shown as an average (* $P \leq 0.05$, Welch's t-test).

5.5 Analysis of autophagic phenotype

Immunostaining of the autophagosome marker microtubule-associated protein 1A/1B-light chain 3 (LC3) in *GRN*$^{+/+}$, *GRN*$^{+/-}$ and *GRN*$^{-/-}$ cells revealed a higher number of autophagosomes in absence of PGRN (Fig.18A). This result was confirmed by HCS quantization of LC3 spots per cell (Fig.18B).

LC3 protein, when located on the autophagosome membrane, is lipidated and called LC3II. *GRN*$^{+/+}$, *GRN*$^{+/-}$ and *GRN*$^{-/-}$ cells were starved 1h with HBSS (inducing the autophagic flux) or treated for 1h with Bafilomycin A1 (BafA1), a specific inhibitor of the vacuolar type H^+-ATPase (V-ATPase) located to the lysosomes. BafA1 inhibits the acidification of organelles and subsequent autophogosomes-lysosomes fusion[153]. Detection of LC3II by WB revealed that

GRN$^{-/-}$ cells show a higher number of autophagosomes than the wt cells when starved or treated with BafA1. In *GRN*$^{+/-}$ cells, instead, there is a reduction of the autophagosomes amount in both conditions compared to *GRN*$^{+/+}$ cells (Fig.19).

In order to analyse the levels of autophagosome-lysosome fusion, *GRN*$^{+/+}$, *GRN*$^{+/-}$ and *GRN*$^{-/-}$ cells were transfected with a plasmid expressing LC3 protein fused to the Green Fluorescent Protein (GFP) and the Red Fluorescent Protein (RFP). GFP is a stably folded protein resistant to lysosomal proteases, but the low pH inside lysosomes quenches its fluorescent signal. In contrast, RFP exhibits a more stable fluorescence in acidic compartments allowing the detection of the red signal into the autolysosomes[121]. Transfected cells were not treated and treated with HBSS or Bafilomycin A1 as positive (induction of autophagy and increased autophagosomes-lysosome fusion) and negative (block of autophagosomes-lysosome fusion) controls respectively. Results reported in Fig.20 underline a reduced autolysosomes formation in *GRN*$^{+/-}$ cells and a block of autophagosomes-lysosomes fusion in *GRN*$^{-/-}$ cells with respect to wt cells.

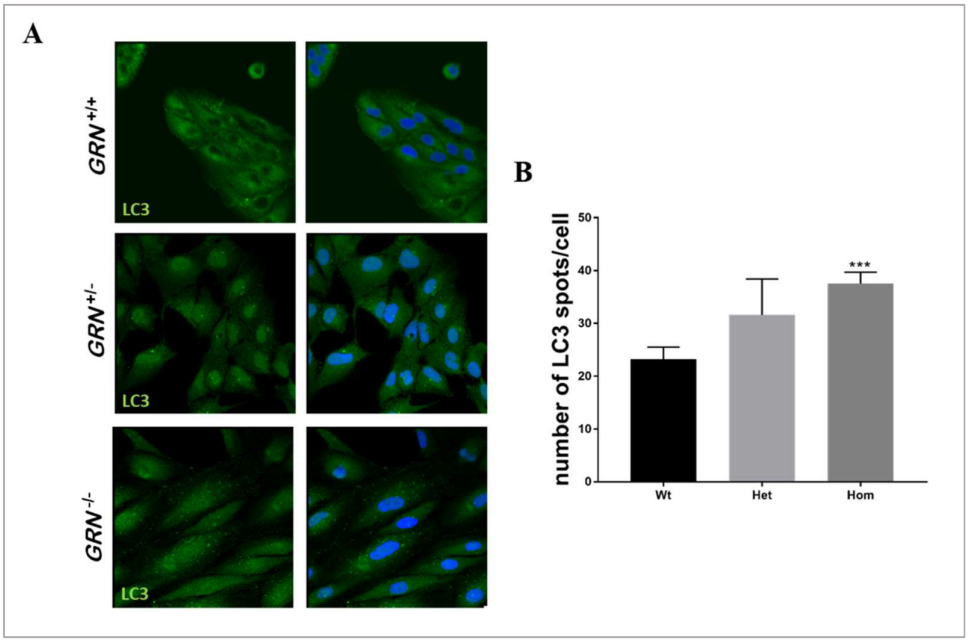

Fig.18 Amount of autophagosomes related to PGRN dosage. (A) Immunostaining of LC3 (green) showing an increased number of LC3 spots in *GRN* KO cells. (B) HCS analysis reporting the number of LC3 spots/cell. Wild type (Wt), heterozygous (Het), homozygous (Hom). Values are shown as an average (*** $P \leq 0.001$, Welch's t-test).

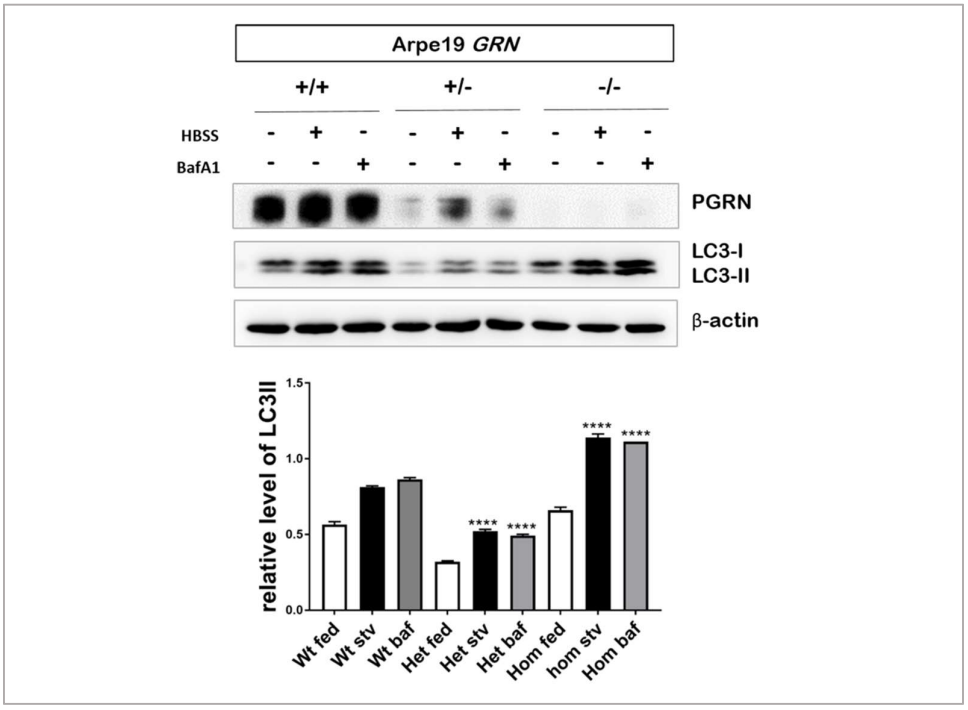

Fig.19 Analysis of autophagic induction. $GRN^{+/+}$, $GRN^{+/-}$ and $GRN^{-/-}$ cells were treated with HBSS (nutrient privation) or 100 nM Bafilomycin A1 (BafA1) for 1h. Western blot assay of LC3II protein shows reduced autophagosomes formation in $GRN^{+/-}$ cells and an increased autophagosomes amount in $GRN^{-/-}$ cells with respect to wt cells, after starvaion and BafA1 treatment. Wild type (Wt), heterozygous (Het), homozygous (Hom). Graph shows densitometry analysis of the Western blot bands. Values are normalized to actin and are shown as an average (*** $P \leq 0.001$, **** $P \leq 0.0001$, Welch's t-test).

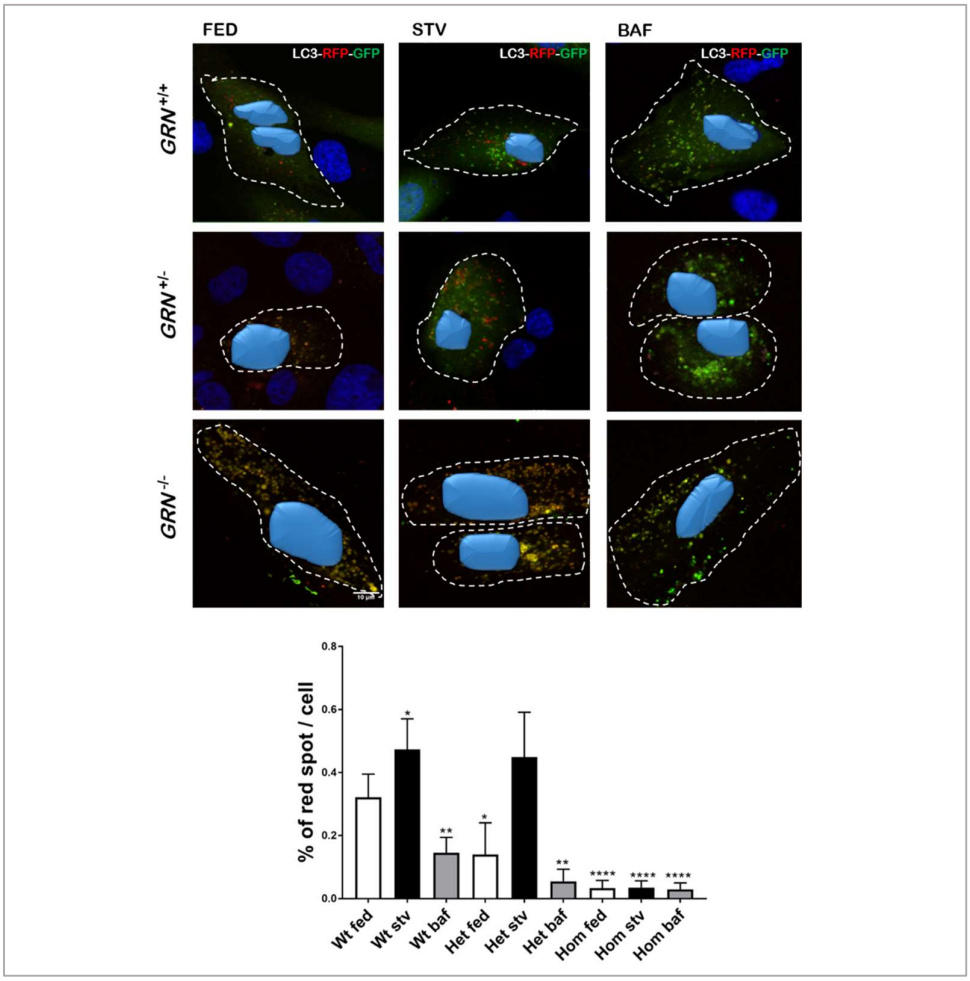

Fig.20 Autophagosomes-lysosomes fusion assay. *GRN*$^{+/+}$, *GRN*$^{+/-}$ and *GRN*$^{-/-}$ cells transfected with LC3-RFP-GFP were not treated (fed) and treated with HBSS (stv) or 100 nM Bafilomycin A1 (baf) for 1h. Yellow dots are representative of autophagosomes, red dots of autolysosomes. Graph reports the percentage of red dots per cell. Wild type (Wt), heterozygous (Het), homozygous (Hom). Values are normalized to number of total spots per cell and are shown as an average (* $P \leq 0.05$, ** $P \leq 0.01$, **** $P \leq 0.0001$, Welch's t-test).

5.6 mTORC1 signalling

mTORC1 activity in *GRN* edited cells was assayed by WB experiments in which the phosphorylation levels of its targets were detected. Eukaryotic translation initiation factor 4E-Binding Protein 1 (4EBP1) and TFEB are mTORC1 kinase substrates, which modulate their activity through translational

modifications. WB results show a decreased 4EBP1 and TFEB phosphorylation in *GRN*$^{+/-}$ and *GRN*$^{-/-}$ cells when compared to wt cells. Moreover, *GRN* heterozygous and homozygous clones showed an increased level of TFEB protein (Fig.21).

Once dephosphorylated, TFEB migrates into the nucleus where it activates the transcription of its targets. To test the transcriptional activation of TFEB targets, a Real Time qPCR was performed on cDNAs derived from mRNAs of *GRN*$^{+/+}$, *GRN*$^{+/-}$ and *GRN*$^{-/-}$ cells. Results reported in Fig.22 display higher transcriptional levels of TFEB itself and of its targets (MCOLN1, WIPI and ATP6VoE1) in *GRN* heterozygous and homozygous conditions, confirming a lower level of phosporylated TFEB and its subsequent traslocation into the nucleus.

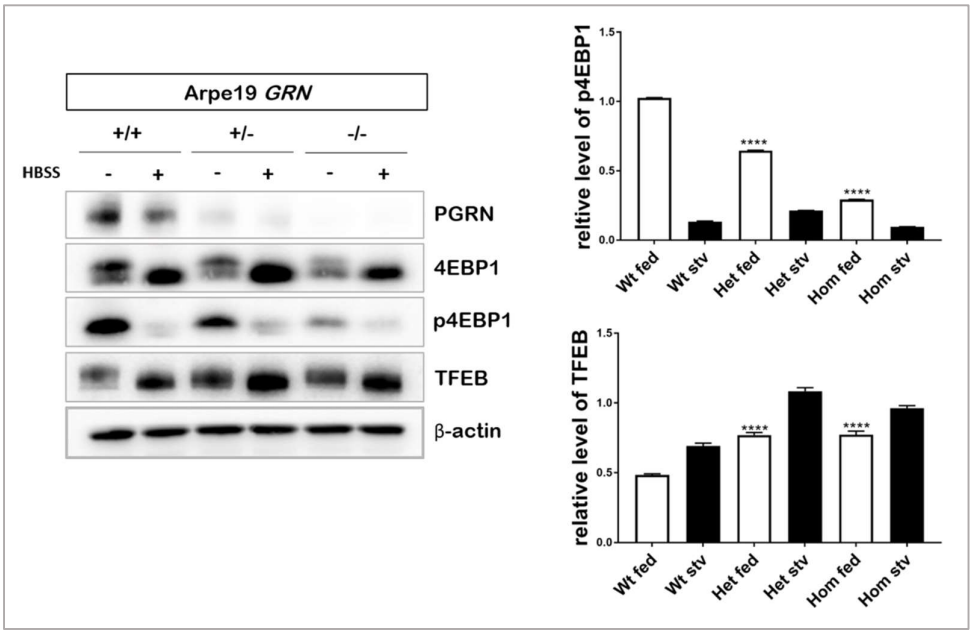

Fig.21 PGRN dependent mTORC1 activity. *GRN*$^{+/+}$, *GRN*$^{+/-}$ and *GRN*$^{-/-}$ cells were not treated (fed) and treated with 1h HBSS (stv) as negative control. In absence of nutrients mTORC1 is inactive and does not phosphorylates its targets. Western blot analysis shows a decreased phosphorylation of 4EBP1 and TFEB in *GRN*$^{+/-}$ and *GRN*$^{-/-}$ cell lines with respect to wt cells. Wild type (Wt), heterozygous (Het), homozygous (Hom). Graph shows densitometry analysis of the Western blot bands. Values are normalized to actin and are shown as an average (**** $P \leq 0.0001$, Welch's t-test).

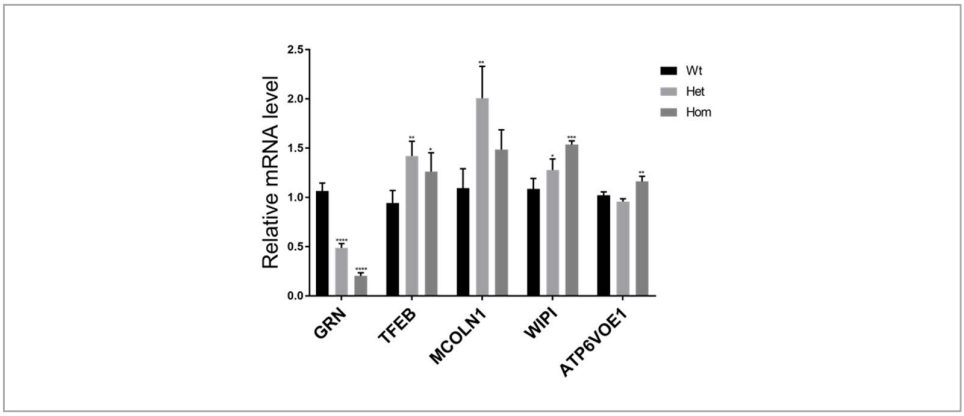

Fig.22 TFEB targets relative mRNA levels. Real time qPCR of TFEB targets (TFEB, MCOLN1, WIPI and ATP6V0E1) in *GRN*$^{+/+}$ (Wt), *GRN*$^{+/-}$ (Het) and *GRN*$^{-/-}$ (Hom) cells revealed that in *GRN* edited cells there is an enhanced transcriptional activation of TFEB targets with respect to wt cells. Values reported in graph are shown as an average (* $P \leq 0.05$, ** $P \leq 0.01$, *** $P \leq 0.001$, **** $P \leq 0.0001$, Welch's t-test).

6. Discussion

NCL11 is an autosomal recessive adulthood neurodegenative disease caused by homozygous null mutations in *GRN* gene[94] and characterized by the lysosomal accumulation of autofluorescent material[15,16,109]. Recent reports show that *GRN* deficiency leads to lysosomal dysfunction through accumulation of abnormal autofluorescent lipopigments[72,114], even though, the mechanism by which this protein acts at the lysosomes, and how its dysfunction leads to NCL11 diseases, is still not known. This lack of knowledge makes it difficult to apply any good therapy to ameliorate patient condition and to stop disease progression.

The starting point to study protein functions and dysfunction in pathological conditions, is to generate a good model system resembling the disease of interest. Currently, in order to investigate the role of *GRN*, different NCL11 model systems, like *GRN* deficient mice[72,76,112,154,155] and primary cultures of *GRN* KO mice derived cells[72,73], have been generated. Thanks to these models, many of the *GRN* functions have been clarified, but its role in regulating lysosomal metabolism is still not clear and a good therapy for NCL11 is far to be applied. One of the main features of all the models available to study NCL11, is the high level of variability, that makes them not suitable candidates for experiments of drugs discoveries by HCS, which require an highly homogeneous cell population. For this reason, the main purpose of this work was to generate a new NCL11 cellular model able to reproduce the disease phenotype and suitable for both cell biology and biochemical approaches, in order to clarify the specific role of *GNR* within lysosomes, and to perform HCS experiments, such as drugs discovery.

Few years ago a new efficient technology of genome editing, the CRISPR-Cas9 system, emerged from the engineering of *S. pyogenes* immunity system. Through this approach, I was able to edit *GRN* gene in Arpe19 cells. This cell line was chosen because retinal dystrophy and retina lipofuscin accumulation

occur in NCL11 patients and mice models[109,110,156]. Obtained *GRN* KO cells displayed lipids storage in the lysosomes, validating this cellular system as a suitable *in vitro* model for NCL11. Instead, lipids accumulation, as expected, was not observed in *GRN*$^{+/-}$ cell line, since *GRN* heterozygous null mutations lead to a non-lysosomal storage disease. Furthermore, despite lipofuscin autofluorescent lipopigments were detected in retina of *GRN*$^{-/-}$ mice[157], they were impossible to be observed in *GRN* KO cells, probably due to cellular division related-dilution.

The concept of LSDs as "autophagy disorders" has emerged in the last years[158] since lysosomes play a key role in the autophagic pathway, by fusing with autophagosomes and digesting their content. Considering the highly integrated function of lysosomes and autophagosomes, it was reasonable to expect that lysosomal storage in LSDs would have an impact upon autophagy [115-117]. In fact, an accelerated storage of the ubiquitinated proteins and of the aging pigment lipofuscin, that normally accumulates in brain during aging, in NCL11 mice models[72,112,114,159], suggests an impairment in the autophagic-lysosomal degradation machinery. Therefore, I investigated the effect of *GRN* haploinsufficiency and depletion on the autophagic pathway in my cellular models. By different approaches, I revealed a higher number of autophagosomes in *GRN*$^{-/-}$ Arpe19 cells than in wt cells. Since the autophagosome is an intermediate structure in a dynamic process, the simple mesurement of the numbers of autophagosomes was not sufficient for a general estimation of the autophagic activity[121]. For this reason, I performed experiments of modulation of the autophagic flux to evaluate the autophagic levels, revealing an increase in *GRN*$^{-/-}$ and a reduction in *GRN*$^{+/-}$ conditions. Wils H. *et al.* observed, in brain of *GRN*$^{-/-}$ mice, more p62-positive inclusions than wt mice[112]. p62 is an autophagosome related protein, which binds LC3 protein on one side, and the ubiquitinated cargo, that must be degraded, on the other side. Once the fusion between autophagosomes and lysosomes occurs, p62 protein is degraded by lysosomal proteases together with the cargo[160]. Increase of p62 inclusions in *GRN*$^{-/-}$ mice brain suggests a damage in

autophagosome-lysosome fusion. The NCL11 cellular model system that I generated confirmed the autophagosome-lysosome fusion impairment and this finding, together with the enhanced autophagic activity, explains the increase in the number of autophagosomes in *GRN* KO cells.

Another important observation was the different cellular phenotypes in *GRN* haploinsufficiency and KO conditions. In fact, through immunofluorescence experiments and a specific script designed to perform HCS quantification, I revealed a higher number of lysosomes in $GRN^{-/-}$ cells than $GRN^{+/-}$ and wt cells. Moreover, to further demonstrate the potency of this tool as a good candidate for HCS and drug discovery experiments, a quantification of the lysosomal distribution was performed in these cell lines. Obtained results revealed that, while Arpe19 wt cells display a uniform lysosomal distribution into the cytosol, $GRN^{+/-}$ cells present a lysosomal perinuclear aggregation, and, in contrast, $GRN^{-/-}$ cells show a higher number of lysosomes located to the plasma membrane. Electron Microscopy experiments indicate that lysosomes show a bigger size in $GRN^{-/-}$ cells than in wt. Furthermore, I evinced an impaired lysosomal trafficking in *GRN* edited cells (data not shown), confirming a direct or indirect role of PGRN (or related-granulins) in lysosome movement, localization and subsequent function.

An important player in the regulation of the autophagic process and lysosomal metabolism is the nutrient-responsive kinase mTOR. Defects in the autophagic-lysosomal pathway, due to abnormal mTORC1 activation, are reported in several LSDs[124]. Tanaka Y. *et al.* demonstrated an impairment in mTORC1 activity in cerebral cortex of PGRN-deficient mice[161]. Thus, a slight reduction of the kinase complex activity in $GRN^{+/-}$ cells and a remarkable inactivation in $GRN^{-/-}$ cells, further confirmed the potency of $GRN^{-/-}$ Arpe19 cell line as a good *in vitro* model system for NCL11. Phosphorylation/ dephosphorylation status of the mTORC1 substrate, TFEB, is an important regulatory mechanism for its activation. Since I found that in $GRN^{-/-}$ and $GRN^{+/-}$ cells the levels of TFEB phosphorilation were less than in wt cells, to confirm

the activation status of TFEB, I performed real time PCR experiments to analyze the expression levels of TFEB target genes. As expected, I found enhanced transcriptional levels of some TFEB target genes, confirming that in these cell lines TFEB is constitutively activated.

It has been demonstated that secreted PGRN interacts with the membrane receptor Sortilin, inducing endocytosis and transport of PGRN to the lysosome[92]. Tanaka Y. *et al.* suggested that the lysosomal localization of PGRN is related to its possible involvement in mTORC1 activation and subsequent cytosolic TFEB retention[161]. Through my *GRN* KO cell model system I could confirm the role of *GRN* in regulating mTORC1 activity. Moreover, Sardiello M. *et al.* demonstrated that in cells derived from LSDs mice there is a predominant nuclear localization of TFEB, suggesting that, after intralysosomal storage of undegraded material, TFEB pathway is activated as a cellular response to enhance cellular clearance[124]. This model is reproduced in *GRN* KO cells, even if it is evident that the enhanced autophagic-lysosomal pathway alone is not able to lead cell clearance. The persistency of the cell phenotype could be due to the fusion defect between autophagosome and lysosomes that makes the "clearance" strategy adopted by the cell uneffective. Strikingly, *GRN* by itself is a target gene of the active TFEB, thus underlining a main role of PGRN in lysosomal function.

In conclusion, by this work I generated a new and reliable model system for NCL11 through the innovative technology of genome editing, the CRISPR-Cas9 system. I obtained and characterized the $GRN^{+/-}$ and $GRN^{-/-}$ Arpe19 cell lines, highlighting the damaged lysosomal and autophagic pathways and pointing out the attention on the different phenotypes related to PGRN dosage, which reflects the onset of two independent diseases in cases of heterozygous or homozygous null mutations in *GRN* gene. These cellular models are good candidates for experiments of HCS thanks to the abolition of variability that occurs using primary cell cultures. Thus, these cell lines allow experiments of drug screening aimed to the detection of new compounds able to revert the

disease phenotype and that could lead to the development of a suitable and reliable therapy to stop the disease progression.

7. Bibliography

1. de Duve C. (2005) The lysosome turns fifty. Nat. Cell Biol. 7, 847–849.
2. Boustany R.M. (2013) Lysosomal storage diseases--the horizon expands. Nat. Rev. Neurol. 9, 583–598.
3. Huizing M., Helip-Wooley A., Westbroek W., Gunay-Aygun M. & Gahl W.A. (2008) Disorders of lysosome-related organelle biogenesis: clinical and molecular genetics. Annu. Rev. Genomics Hum. Genet. 9, 359–386.
4. Hers H. G. (1965) Inborn lysosomal diseases. Gastroenterology 48, 625–633.
5. Ballabio A. & Gieselmann V. (2009) Lysosomal disorders: from storage to cellular damage. Biochim. Biophys. Acta 1793, 684–696.
6. Filocamo M. & Morrone A. (2011) Lysosomal storage disorders: Molecular basis and laboratory testing. Human Genomics. Vol 5. No 3, 156–169.
7. Jalanko A. and Braulke T. (2009) Neuronal ceroid lipofuscinoses. Biochim. Biophys. Acta Vol. 1793, 697–709.
8. Haltia M. (2006) The neuronal ceroid lipofuscinoses: from past to present. Biochim. Biophys. Acta Vol. 1762, 850-856.
9. Goebel H.H., Mole S., Lake B.D. (1999) The Neuronal Ceroid Lipofuscinoses (Batten Disease). IOS Press, Amsterdam, pp. 1-197.
10. Mink J.W., Augustine E.F., Adams H.R., Marshall F.J., Kwon J.M. (2013) Classification and natural history of the neuronal ceroid lipofuscinoses. J. Child Neurol., 28, 1101−5.
11. Haltia M., Goebel H.H. (2013) The neuronal ceroid-lipofuscinoses: A historical introduction. Biochim. Biophys. Acta, Mol. Basis Dis. 1832, 1795−800.
12. Schulz A., Kohlschutter A., Mink J., Simonati A., Williams R. (2013) NCL diseases - clinical perspectives. Biochim. Biophys. Acta, Mol. Basis Dis. 1832, 1801−6.
13. Lockhart E.M., Warner D.S., Pearlstein R.D., Penning D.H., Mehrabani S., Boustany R.M. (2002) Allopregnanolone attenuates N- methyl-D-aspartate-induced excitotoxicity and apoptosis in the human NT2 cell line in culture. Neurosci. Lett. 328, 33−36.
14. Persaud-Sawin D.A., Boustany R.M. (2005) Cell death pathways in juvenile Batten disease. Apoptosis 10, 973−85.
15. Anderson G.W., Goebel H.H., Simonati A. (2013) Human pathology in NCL. Biochim. Biophys. Acta, Mol. Basis Dis. 1832, 1807−26.
16. Palmer D.N., Barry L.A., Tyynela J., Cooper J.D. (2013) NCL disease mechanisms. Biochim. Biophys. Acta, Mol. Basis Dis. 1832, 1882−93.

17. Boustany R.M. (2013) Lysosomal storage diseases- the horizon expands. Nat. Rev. Neurol. 9, 583−98.
18. Carcel-Trullols J., Kovacs A.D., Pearce D.A. (2015) Cell biology of the NCL proteins: What they do and don't do. Biochim. Biophys. Acta, Mol. Basis Dis. 1852, 2242−55.
19. Mole S.E., Cotman S.L. (2015) Genetics of the neuronal ceroid lipofuscinoses (Batten disease). Biochim. Biophys. Acta, Mol. Basis Dis. 1852, 2237−41.
20. Rakheja D., Narayan S.B., Bennett M.J. (2008) The function of CLN3P, the Batten disease protein. Mol. Genet. Metab. 93, 269− 74.
21. Rakheja D., Narayan S.B., Bennett M.J. (2007) Juvenile neuronal ceroid-lipofuscinosis (Batten disease): A brief review and update. Curr. Mol. Med. 7, 603−8.
22. Phillips S.N., Benedict J.W., Weimer J.M., Pearce D.A. (2005) CLN3, the protein associated with Batten disease: Structure, function and localization. J. Neurosci. Res. 79, 573−83.
23. Lin L., Sohar I., Lackland H., Lobel P. (2001) The human CLN2 protein/tripeptidyl-peptidase I is a serine protease that autoactivates at acidic pH. J. Biol. Chem. 276, 2249−55.
24. Vesa J., Hellsten E., Verkruyse L.A., Camp L.A., Rapola J., Santavuori P., Hofmann S.L., Peltonen L. (1995) Mutations in the palmitoyl protein thioesterase gene causing infantile neuronal ceroid lipofuscinosis. Nature 376, 584−7.
25. Camp L.A., Hofmann S.L. (1993) Purification and properties of a palmitoyl-protein thioesterase that cleaves palmitate from H-Ras. J. Biol. Chem. 268, 22566−74.
26. Noskova L., Stranecky V., Hartmannova H., Pristoupilova A., Baresova V., Ivanek R., Hulkova H., Jahnova H., van der Zee J., Staropoli J.F., Sims K.B., Tyynela J., Van Broeckhoven C., Nijssen P.C., Mole S.E., Elleder M., Kmoch S. (2011) Mutations in DNAJC5, encoding cysteine-string protein alpha, cause autosomal-dominant adult-onset neuronal ceroid lipofuscinosis. Am. J. Hum. Genet. 89, 241−52.
27. Mastrogiacomo A., Parsons S.M., Zampighi G.A., Jenden D.J., Umbach J.A., Gundersen C.B. (1994) Cysteine string proteins: A potential link between synaptic vesicles and presynaptic Ca2+ channels. Science 263, 981−82.
28. Sharma M., Burre J., Sudhof T.C. (2011) CSP [alpha] promotes SNARE-complex assembly by chaperoning SNAP-25 during synaptic activity. Nat. Cell Biol. 13, 30 −39.
29. Kollmann K., Uusi-Rauva K., Scifo E., Tyynela J., Jalanko A., Braulke T. (2013) Cell biology and function of neuronal ceroid lipofuscinosis- related proteins. Biochim. Biophys. Acta, Mol. Basis Dis. 1832, 1866−81.
30. Smith K.R., Dahl H.H.M., Canafoglia L., Andermann E., Damiano J., Morbin M., Bruni A.C., Giaccone G., Cossette P., Saftig P., Grötzinger J., Schwake M.,

Andermann F., Staropoli J.F., Sims K.B., Mole S.E., Franceschetti S., Alexander N.A., Cooper J.D., Chapman H.A., Carpenter S., Berkovic S.F., Bahlo M. (2013) Cathepsin F mutations cause Type B Kufs disease, an adult-onset neuronal ceroid lipofuscinosis. Hum. Mol. Genet. 22, 1417−23.

31. Mole S., Williams R. & Goebel H. (Eds) The Neuronal Ceroid Lipofuscinoses, Batten Disease (Oxford University Press, 2012).
32. Schulz A., Dhar S., Rylova S., Dbaibo G., Alroy J., Hagel C., Artacho I., Kohlschutter A., Lin S., Boustany R.M. (2004) Impaired cell adhesion and apoptosis in a novel CLN9 Batten disease variant. Ann. Neurol. 56, 342−50.
33. Vidal-Donet J.M., Carcel-Trullols J., Casanova B., Aguado C., Knecht E. (2013) Alterations in ROS activity and lysosomal pH account for distinct patterns of macroautophagy in LINCL and JNCL fibroblasts. PLoS One 8, e55526.
34. Sleat D.E., Gin R.M., Sohar I., Wisniewski K., Sklower- Brooks S., Pullarkat R.K., Palmer D.N., Lerner T.J., Boustany R.M., Uldall P., Siakotos A.N., Donnelly R.J., Lobel P. (1999) Mutational analysis of the defective protease in classic late-infantile neuronal ceroid lipofuscinosis, a neurodegenerative lysosomal storage disorder. Am. J. Hum. Genet. 64, 1511−23.
35. Lu J.Y., Hofmann S.L. (2006) Inefficient cleavage of palmitoyl- protein thioesterase (PPT) substrates by aminothiols: Implications for treatment of infantile neuronal ceroid lipofuscinosis. J. Inherited Metab. Dis. 29, 119−26.
36. Sarkar C., Chandra G., Peng S., Zhang Z., Liu A., Mukherjee A.B. (2013) Neuroprotection and lifespan extension in Ppt1(−/−) mice by NtBuHA: Therapeutic implications for INCL. Nat. Neurosci. 16, 1608−17.
37. Kim J.B., Lim N., Kim S.J., Heo T.H. (2012) N-acetylcysteine normalizes the urea cycle and DNA repair in cells from patients with Batten disease. Cell Biochem. Funct. 30, 677−82.
38. Narayan S.B., Rakheja D., Tan L., Pastor J.V., Bennett M.J. (2006) CLN3P, the Batten's disease protein, is a novel palmitoyl-protein Delta-9 desaturase. Ann. Neurol. 60, 570−7.
39. Nihar Kinarivala and Paul C. Trippier. (2016) Progress in the Development of Small Molecule Therapeutics for the Treatment of Neuronal Ceroid Lipofuscinoses (NCLs). J. Med. Chem. 59 (10), 4415–4427.
40. Tamaki S.J., Jacobs Y., Dohse M., Capela A., Cooper J.D., Reitsma M., He D., Tushinski R., Belichenko P.V., Salehi A., Mobley W., Gage F.H., Huhn S., Tsukamoto A.S., Weissman I.L., Uchida N. (2009) Neuroprotection of host cells by human central nervous system stem cells in a mouse model of infantile neuronal ceroid lipofuscinosis, Cell Stem Cell 5 (3) 310-319.

41. Cooper J.D., Russell C., Mitchison H.M. (2006) Progress towards understanding disease mechanisms in small vertebrate models of neuronal ceroid lipofuscinosis, Biochim. Biophys. Acta 1762 (10) 873-889.
42. Jolly R.D., Martinus R.D., Palmer D.N. (1992) Sheep and other animals with ceroid-lipofuscinoses: their relevance to Batten disease, Am. J. Med. Genet. 42 (4) 609-614.
43. Nevermana N.J., Besta H.L.,. Hofmannc S.L., Hughes S.M. (2015) Experimental therapies in the neuronal ceroid lipofuscinoses, Biochim. Biophys. Acta, Mol. Basis Dis. 1852, 2292–2300.
44. Schiffmann R., Heyes M.P., Aerts J.M., Dambrosia J.M., Patterson M.C., DeGraba T., Parker C.C., Zirzow G.C., Oliver K., Tedeschi G., Brady R.O., Barton N.W. (1997) Prospective study of neurological responses to treatment with macrophage-targeted glucocerebrosidase in patients with type 3 Gaucher's disease, Ann. Neurol. 42 (4) 613-621.
45. Sands M.S., Davidson B.L. (2006) Gene therapy for lysosomal storage disease, Mol. Ther. 13 (5) 839-849.
46. Lonnqvist T., Vanhanen S.L., Vettenranta K., Autti T., Rapola J., Santavuori P., Saarinen-Pihkala U.M. (2001) Hematopoietic stem cell transplantation in infantile neuronal ceroid lipofuscinosis, Neurology 57 (8) 1411-1416.
47. Bhandari V., Bateman A. (1992) Structure and chromosomal location of the human granulin gene. Biochem Biophys Res Commun 188:57–63.
48. Bateman A., Bennett H.P. (1998) Granulins: the structure and function of an emerging family of growth factors. J Endocrinol 158:145–151.
49. Hrabal R.,Chen Z., James S., Bennett H.P., and Ni F. (1996) The hairpin stackfold ,a novel protein architecture for a new family of protein growth factors. Nat.Struct. Biol. 3,747–752.
50. Tolkatchev D., Malik S., Vinogradova A., Wang P., Chen Z., Xu P., Bennett H.P., Bateman A., and Ni F. (2008) Structure dissection of human progranulin identifies well folded granulin-epithelin modules with unique functional activities. Protein Sci. 17,711–724.
51. Zhu J., Nathan C., Jin W., Sim D., Ashcroft G.S., Wahl S.M., Lacomis L., Erdjument-Bromage H., Tempst P., Wright C.D., and Ding A. (2002) Conversion of proepithelin to epithelins: roles of SLPI and elastase in host defense and wound repair. Cell 111, 867–878.
52. Suh H.S., Choi N., Tarassishin L., and Lee S.C. (2012) Regulation of progranulin expression in human microglia and proteolysis of progranulin by matrix metalloproteinase 12 (MMP-12). PLoSONE 7, e35115.

53. Butler G.S., Dean R.A., Tam E.M., and Overall C.M. (2008) Pharmacoproteomics of a metalloproteinase hydroxamate inhibitor in breast cancer cells: dynamics of membrane type 1 matrix metalloproteinase-mediated membrane protein shedding. Mol. Cell. Biol. 28, 4896–4914.
54. Bai X.H., Wang D.W., Kong L., Zhang Y., Luan Y., Kobayashi T., Kronenberg H.M., Yu X.P., and Liu C.J. (2009) ADAMTS-7, a direct target of PTHrP, adversely regulates endochondral bone growth by associating with and inactivating GEP growth factor. Mol. Cell. Biol. 29, 4201–4219.
55. Kessenbrock K., Fröhlich L., Sixt M., Lämmermann T., Pfister H., Bateman A., Belaaouaj A., Ring J., Ollert M., Fässler R., and Jenne D.E. (2008) Proteinase 3 and neutrophil elastase enhance inflammation in mice by inactivating anti-inflammatory progranulin. J. Clin. Invest. 118, 2438–2447.
56. Bateman A., Bennett H.P.J. (2009) The granulin gene family: from cancer to dementia. BioEssays 31:1245-1254.
57. Cadieux B., Chitramuthu B.P., Baranowski D., Bennett H.P. (2005) The zebrafish progranulin gene family and antisense transcripts. BMC Genomics 6:156.
58. Plowman G.D., Green J.M., Neubauer M.G., Buckley S.D., McDonald V.L., Todaro G.J., Shoyab M. (1992) The epithelin precursor encodes two proteins with opposing activities on epithelial cell growth. J. Biol. Chem. 267: 13073-13078.
59. Baba T., Hoff H.B., Nemoto H., Lee H., Orth J., Arai Y., Gerton G.L. Acrogranin, an acrosomal cysteine-rich glycoprotein, is the precursor of the growth-modulating peptides, granulins, and epithelins, and is expressed in somatic as well as male germ cells. Molec. Reprod. Dev. 34: 233-243.
60. Serrero, G. (2003) Autocrine growth factor revisited: PC-cell-derived growth factor (progranulin), a critical player in breast cancer tumorigenesis. Biochem. Biophys. Res. Commun. 308: 409-413.
61. Parnell P.G., Wunderlich J., Carter B., Halper J. (1992) Transforming growth factor e: amino acid analysis and partial amino acid sequence. Growth Factors 7:65–72.
62. Zhou J., Gao G., Crabb J.W., Serrero G. (1993) Purification of an autocrine growth factor homologous with mouse epithelin precursor from a highly tumorigenic cell line. J Biol Chem 268:10863–10869.
63. Bhandari V., Giaid A., Bateman A. (1993) The complementary deoxyribonucleic acid sequence, tissue distribution, and cellular localization of the rat granulin precursor. Endocrinology 133:2682–2689.
64. Bhandari V., Palfree R.G., Bateman A. (1992) Isolation and sequence of the granulin precursor cDNA from human bone marrow reveals tandem cysteine-rich granulin domains. Proc. Natl. Acad. Sci. U.S.A. 89, 1715–1719.

65. Daniel R., He Z., Carmichael K.P., Halper J., Bateman A. (2000) Cellular localization of gene expression for progranulin. J. Histochem. Cytochem. 48,999–1009.
66. Daniel R., Daniels E., He Z., Bateman A. (2003) Progranulin (acrogranin/PC cell-derived growth factor/granulin-epithelin precursor) is expressed in the placenta, epidermis, microvasculature, and brain during murine development. Dev. Dyn. 227, 593–599.
67. Mackenzie I.R., Baker M., Pickering-Brown S., Hsiung G.Y., Lindholm C., Dwosh, E., Gass J., Cannon A., Rademakers R., Hutton M., Feldman H.H. (2006) The neuropathology of frontotemporal lobar degeneration caused by mutations in the progranulin gene. Brain 129, 3081–3090.
68. Matsubara T., Mita A., Minami K., Hosooka T., Kitazawa S., Takahashi K., Tamori Y., Yokoi N., Watanabe M., Matsuo E., Nishimura O., Seino S. (2012) PGRN is a key adipokine mediating high fat diet-induced insulin resistance and obesity through IL-6 in adipose tissue. Cell Metab. 15, 38–50.
69. Petkau T.L., Neal S.J., Orban P.C., MacDonald J.L., Hill A.M., Lu G., Feldman H.H., Mackenzie I.R., Leavitt B.R. (2010) Progranulin expression in the developing and adult murine brain. J Comp Neurol 518:3931–3947.
70. Xu J., Xilouri M., Bruban J., Shioi J., Shao Z., Papazoglou I., Vekrellis K., Robakis N.K. (2011) Extracellular progranulin protects cortical neurons from toxic insults by activating survival signalling. Neurobiol Aging 32:2326.e5-2326.e16.
71. VanDamme P., Van Hoecke A., Lambrechts D., Vanacker P., Bogaert E., van Swieten J., Carmeliet P., Van Den Bosch L., Robberecht W. (2008) Progranulin functions as a neurotrophic factor to regulate neurite outgrowth and enhance neuronal survival. J Cell Biol 181:37–41.
72. Petkau T.L., Neal S.J., Milnerwood A., Mew A., Hill A.M., Orban P., Gregg J., Lu G., Feldman H.H., Mackenzie I.R., Raymond L.A., Leavitt B.R. (2012) Synaptic dysfunction in progranulin-deficient mice. Neurobiol. Dis. 45,711–722.
73. Tapia L., Milnerwood A., Guo A., Mills F., Yoshida E., Vasuta C., Mackenzie, I.R., Raymond L., Cynader M., Jia W., Bamji S.X. (2011) Progranulin deficiency decreases gross neural connectivity but enhances transmission at individual synapses. J. Neurosci. 31, 11126–11132.
74. Cenik B., Sephton C.F., Kutluk Cenik B., Herz J., Yu G. (2012) Progranulin: A Proteolytically Processed Protein at the Crossroads of Inflammation and Neurodegeneration. J. Biol Chem vol 287, 39: 32298-32306.
75. Suzuki M., Bannai M., Matsumuro M., Furuhata Y., Ikemura R., Kuranaga E., Kaneda Y., Nishihara M., Takahashi M. (2000) Suppression of copulatory behavior by

intracerebroventricular infusion of antisense oligodeoxynucleotide of granulin in neonatal male rats. Physiol Behav 68: 707-713.

76. Kayasuga Y., Chiba S., Suzuki M., Kikusui T., Matsuwaki T., Yamanouchi K., Kotaki H., Horai R., Iwakura Y., Nishihara M. (2007). Alteration of behavioural phenotype in mice by targeted disruption of the progranulin gene. Behav Bain Res 185: 110-118.
77. Qin J., Diaz-Cueto L., Schwarze J.E., Takahashi Y., Imai M., Isuzugawa K., Yamamoto S., Chang K.T., Gerton G.L., Imakawa K. (2005). Effect of progranulin on blastocyst hatching and subsequent adhesion and outgrowth in the mouse. Biol Reprod 73: 434-442.
78. Desmarais J.A., Cao M., Bateman A., Murphy B.D. (2008) Spatiotemporal expression pattern of progranulin in embryo implantation and placenta formation suggest a role in cell proliferation, remodelling, and angiogenesis. Reproduction 136:247-257.
79. He Z., Ong C.H., Halper J., Bateman A. (2003) Progranulin is a mediator of the wound response. Nat Med 9: 225-229.
80. Donald C.D., Laddu A., Chandham P., Lim S.D., Cohen C., Amin M., Gerton G.L., Marshall F.F., Petros J.A. (2001) Expression of progranulin and the epithelin/granulin precursor acrogranin correlates with neoplastic state in renal epithelium. Anticancer Res. 21, 3739–3742.
81. Ong C.H., and Bateman A. (2003) Progranulin (granulin-epithelin precursor, PC cell derived growth factor, acrogranin) in proliferation and tumorigenesis. Histol. Histopathol. 18, 1275–1288.
82. Cuevas-Antonio R., Cancino C., Arechavaleta-Velasco F., Andrade A., Barron L., Estrada I., Fernandez R. L., Olguin V., Ruiz S., Imani F., Zeferino-Toquero M., Ulloa-Aguirre A., Gerton G.L., Diaz-Cueto L. (2010) Expression of progranulin (acrogranin/ PCDGF/ granulin-epithelinprecursor) in benign and malignant ovarian tumors and activation of MAPK signalling in ovarian cancer cell line. Cancer Invest. 28, 452–458.
83. Liau L.M., Lallone R.L., Seitz R.S., Buznikov A., Gregg J.P., Kornblum H.I., Nelson S.F., Bronstein J.M. (2000) Identification of a human glioma-associated growth factor gene, granulin, using differential immunoabsorption. Cancer Res. 60, 1353–1360.
84. Matsumura N., Mandai M., Miyanishi M., Fukuhara K., Baba T., Higuchi T., Kariya M., Takakura K., Fujii S. (2006) Oncogenic property of acrogranin in human uterine leiomyosarcoma: direct evidence of genetic contribution in *in vivo* tumorigenesis. Clin. CancerRes. 12, 1402–1411.
85. He Z., Ismail A., Kriazhev L., Sadvakassova G., Bateman A. (2002) Progranulin (PC cell-derived growth factor/acrogranin) regulates invasion and cell survival. Cancer Res. 62, 5590–5596.

86. Monami G. (2006) Proepithelin promotes migration and invasion of 5637 bladder cancer cells through the activation of ERK1/2 and the formation of a paxillin-FAK-ERK complex. Cancer Res. 66, 7103–7110.
87. Feng J.Q., Guo F.J., Jiang B.C., Zhang Y., Frenkel S., Wang D.W., Tang W., Xie Y., Liu C.J. (2010) Granulin-epithelin precursor: a bone morphogenic protein 2-inducible growth factor that activates ERK1/2 signaling and JunB transcription factor in chondrogenesis. FASEB J. 24,1879–1892.
88. Zhu J., Nathan C., Jin W., Sim D., Ashcroft G.S., Wahl S.M., Lacomis L., Erdjument-Bromage H., Tempst P., Wright C.D., Ding A. (2002) Conversion of proepithelin to epithelins: roles of SLPI and elastase in host defense and wound repair. Cell 111:867–878.
89. Tang W., Lu Y., Tian Q.Y., Zhang Y., Guo F.J., Liu G.Y., Syed N.M., Lai Y., Lin E.A., Kong L., Su J., Yin F., Ding A.H., Zanin-Zhorov A., Dustin M.L., Tao J., Craft J., Yin Z., Feng J.Q., Abramson S.B., Yu X.P., Liu C.J. (2011) The growth factor progranulin binds to TNF receptors and is therapeutic against inflammatory arthritis in mice. Science 32:478–484.
90. Okura H., Yamashita S., Ohama T., Saga A., Yamamoto-Kakuta A., Hamada Y., Sougawa N., Ohyama R., Sawa Y., Matsuyama A. (2010) HDL/apolipoprotein A-I binds to macrophage-derived progranulin and suppresses its conversion into proinflammatory granulins. J Atheroscler Thromb 17:568–577.
91. Kessenbrock K., Frohlich L., Sixt M., Lammermann T., Pfister H., Bateman A., Belaaouaj A., Ring J., Ollert M., Fassler R., Jenne D.E. (2008) Proteinase 3 and neutrophil elastase enhance inflammation in mice by inactivating anti-inflammatory progranulin. J Clin Invest 118:2438–2447.
92. Hu F., Padukkavidana T., Vægter B.C., Brady A.O., Zheng Y., Mackenzie R.I., Feldman H.H., Nykjaer A., Strittmatter M.S. (2010) Sortilin-Mediated Endocytosis Determines Levels of the FrontoTemporal Dementia Protein, Progranulin. Neuron . 68(4): 654–667.
93. Willnow T.E., Petersen C.M., Nykjaer A. (2008) VPS10P-domain receptors - regulators of neuronal viability and function. Nat Rev Neurosci 9:899–909.
94. Smith K.R., Damiano J., Franceschetti S., Carpenter S., Canafoglia L., Morbin M., Rossi G., Pareyson D., Mole S.E., Staropoli J.F., Sims K.B., Lewis J., Lin W.L., Dickson D.W., Dahl H.H., Bahlo M., Berkovic, S. F. (2012) Strikingly different clinicopathological phenotypes determined by progranulin mutation dosage. Am. J. Hum. Genet. 90, 1102–1107.
95. Mackenzie I.R., Baker M., Pickering-Brown S., Hsiung G.Y., Lindholm C., Dwosh E., Gass J., Cannon A., Rademakers R., Hutton M., Feldman H.H. (2006) The

neuropathology of frontotemporal lobar degeneration caused by mutations in the progranulin gene. Brain 129, 3081–3090.

96. Ratnavalli E., Brayne C., Dawson K., Hodges J.R. (2002) The prevalence of frontotemporal dementia. Neurology 58, 1615–1621.
97. Rabinovici G.D., and Miller, B.L. (2010) Frontotemporal lobar degeneration: epidemiology, pathophysiology, diagnosis, and management. CNS Drugs 24, 375–398.
98. Gass J., Cannon A., Mackenzie I.R., Boeve B., Baker M., Adamson J., Crook R., Melquist S., Kuntz K., Petersen R., Josephs K., Pickering Brown S.M., Graff-Radford N., Uitti R., Dickson D., Wszolek Z., Gonzalez J., Beach T.G., Bigio E., Johnson N., Weintraub S., Mesulam M., White C. L., Woodruff B., Caselli R., Hsiung G.Y., Feldman H., Knopman D., Hutton M., and Rademakers R. (2006) Mutations in progranulin are a major cause of ubiquitin-positive frontotemporal lobar degeneration. Hum. Mol. Genet. 15, 2988–3001.
99. Rademakers R., Baker M., Gass J., Adamson J., Huey E.D., Momeni P., Spina S., Coppola G., Karydas A.M., Stewart H., Johnson N., Hsiung G.Y., Kelley B., Kuntz K., Steinbart E., Wood E.M., Yu C.E., Josephs K., Sorenson E., Womack K. B., Weintraub S., Pickering-Brown S.M., Schofield P.R., Brooks W.S., Van Deerlin V.M., Snowden J., Clark C.M., Kertesz A., Boylan K., Ghetti B., Neary D., Schellenberg G.D., Beach T.G., Mesulam M., Mann D., Grafman J., Mackenzie I.R., Feldman H., Bird T., Petersen R., Knopman D., Boeve B., Geschwind D.H., Miller B., Wszolek Z., Lippa C., Bigio E.H., Dickson D., Graff-Radford N., Hutton M. (2007) Phenotypic variability associated with progranulin haploinsufficiency in patients with the common 1477C -T (Arg493X) mutation: an international initiative. Lancet Neurol. 6, 857–868.
100. van Swieten J.C., Heutink P. (2008) Mutations in progranulin (GRN) within the spectrum of clinical and pathological phenotypes of frontotemporal dementia. Lancet Neurol 7:965–9.
101. Arai T., Hasegawa M., Akiyama H., Ikeda K., Nonaka T., Mori H., Mann D., Tsuchiya K., Yoshida M., Hashizume Y., Oda T. (2006) TDP-43 is a component of ubiquitin-positive tau-negative inclusions in frontotemporal lobar degeneration and amytrophic lateral sclerosis. Biochem Biophys Res Commun 351: 602-611.
102. Neumann M., Sampathu D.M., Kwong L.K., Truax A.C., Micsenyi M.C., Chou T.T., Bruce J., Schuck T., Grossman M., Clark C. M., McCluskey L.F., Miller B.L., Masliah E., Mackenzie I.R., Feldman H., Feiden W., Kretzschmar H.A., Trojanowski J.Q., and Lee V.M. (2006) Ubiquitinated TDP-43 in frontotemporal lobar degeneration and amyotrophic lateral sclerosis. Science 314, 130–133.
103. Sephton C.F., Cenik C., Kucukural A., Dammer E.B., Cenik B., Han Y., Dewey C.M., Roth F.P., Herz J., Peng J., Moore M.J., and Yu G. (2011) Identification of neuronal

RNA targets of TDP-43-containing ribonucleoprotein complexes. J. Biol. Chem. 286, 1204–1215.

104. Colombrita C., Onesto E., Megiorni F., Pizzuti A., Baralle F.E., Buratti E., Silani V., and Ratti A. (2012) TDP-43 and FUS RNA-binding proteins bind distinct sets of cytoplasmic messenger RNAs and differently regulate their post-transcriptional fate in motoneuron-like cells. J. Biol. Chem. 287, 15635–15647.
105. Gass J., Cannon A., Mackenzie I.R., Boeve B., Baker M., Adamson J., Crook R., Melquist S., Kuntz K., Petersen R., Josephs K., Pickering-Brown S.M., Graff-Radford N., Uitti R., Dickson D., Wszolek Z., Gonzalez J., Beach T.G., Bigio E., Johnson N., Weintraub S., Mesulam M., White C.L., Woodruff B., Caselli R., Hsiung G.Y., Feldman H., Knopman D., Hutton M., Rademakers R. (2006) Mutations in progranulin are a major cause of ubiquitin-positive frontotemporal lobar degeneration. Hum Mol Genet 15: 2988-3001.
106. Le Ber I., van der Zee J., Hannequin D., Gijselinck I., Campion D., Puel M., Laquerriere A., De Pooter T., Camuzat A., Van den Broeck M., Dubois B., Sellal F., Lacomblez L., Vercelletto M., ThomasAnterion C., Michel B.F., Golfier V., Didic M., Salachas F., Duyckaerts C., Cruts M., Verpillat P., Van Broeckhoven C., Brice A. (2007) Progranulin null mutations in both sporadic and familial frontotemporal dementia. Hum Mutat 28:846–855.
107. Gijselinck I., van der Zee J., Engelborghs S., Goossens D., Peeters K., Mattheijssens M., Corsmit E., Del-Favero J., De Deyn P.P., Van Broeckhoven C., Cruts M. (2008) Progranulin locus deletion in frontotemporal dementia. Hum Mutat 29:53–58.
108. Rovelet-Lecrux A., Deramecourt V., Legallic S., Maurage C.A., Le B.I., Brice A., Lambert J.C., Frebourg T., Hannequin D., Pasquier F., Campion D. (2008) Deletion of the progranulin gene in patients with frontotemporal lobar degeneration or Parkinson disease. Neurobiol Dis 31:41–45.
109. Jung T., Bader N., Grune T. (2007) Lipofuscin: formation, distribution, and metabolic consequences. Ann. N.Y. Acad. Sci. 1119, 97–111.
110. Canafoglia L., Morbin M., Scaioli V., Pareyson D., D'Incerti L., Fugnanesi V., Tagliavini F., Berkovic S.F., Franceschetti S. (2014) Recurrent generalized seizures, visual loss, and palinopsia as phenotypic features of neuronal ceroid lipofuscinosis due to progranulin gene mutation. Epilepsia 55(6):e56-e59.
111. Carpenter S., Karpati G., Andermann F., Jacob J.C., Andermann E. (1977). The ultrastructural characteristics of the abnormal cytosomes in Batten-Kufs' disease. Brain 100, 137-156.
112. Wils H., Kleinberger G., Pereson S., Janssens J., Capell A., Van Dam D., Cuijt I., Joris G., De Deyn P.P., Haass C., Van Broeckhoven C., Kumar-Singh S. (2012) Cellular

ageing, increased mortality and FTLD-TDP-associated neuropathology in progranulin knockout mice. J Pathol 228(1):67–76.

113. Kleinberger G., Capell A., Haass C., Van Broeckhoven C. (2013) Mechanism of granulin deficiency: lessons from cellular and animal models. Mol Neurobiol 47: 337-360.
114. Ahmed Z., Sheng H., Xu Y.F., Lin W.L., Innes A.E., Gass J., Yu X., Hou H., Chiba S., Yamanouchi K., Leissring M., Petrucelli L., Nishihara M., Hutton M.L., McGowan E., Dickson D.W., Lewis J. (2010) Accelerated lipofuscinosis and ubiquitination in granulin knockout mice suggests a role for progranulin in successful aging. Am J Pathol 177:311–324.
115. Levine B., and Kroemer G. (2008) Autophagy in the pathogenesis of disease. Cell 132, 27-42.
116. Mizushima N., Levine B., Cuervo A.M., Klionsky D.J. (2008) Autophagy fights disease through cellular self-digestion. Nature 451, 1069-1075.
117. Rubinsztein D.C. (2006) The roles of intracellular protein-degradation pathways in neurodegeneration. Nature 443, 780-786.
118. Kiriyama Y. and Nochi H. (2015) The function of autophagy in neurodegenerative disease. J. Mol. Scien 16, 26797-26812.
119. Hara T., Nakamura K., Matsui M., Yamamoto A., Nakahara Y., Suzuki-Migishima R., Yokoyama M., Mishima K., Saito I., Okano H., Mizushima N. (2006) Suppression of basal autophagy in neural cells causes neurodegenerative disease in mice. Nature 441, 885–889.
120. Komatsu M., Waguri S., Chiba T., Murata S., Iwata J., Tanida I., Ueno T., Koike M., Uchiyama Y., Kominami E., Tanaka K. (2006) Loss of autophagy in the central nervous system causes neurodegeneration in mice. Nature 441, 880–884.
121. Mizushima N., Yoshimori T., Levine B. (2010) Methods in mammalian autophagy research. Cell 140(3): 313-26.
122. Settembre C., Di Malta C., Polito V.A., Garcia Arencibia M., Vetrini F., Erdin S., Erdin S.U., Huynh T., Medina D., Colella P., Sardiello M., Rubinsztein D.C., Ballabio A. (2011) TFEB links autophagy to lysosomal biogenesis. Science. 332:1429–33.
123. Steingrímsson E., Copeland N.G. and Jenkins N.A. (2004) Melanocytes and the microphthalmia transcription factor network. Annu. Rev. Genet. 38, 365-411.
124. Sardiello M., Palmieri M., di Ronza A., Medina D.L., Valenza M., Gennarino V.A., Di Malta C., Donaudy F., Embrione V., Polishchuk R.S., Banfi S., Parenti G., Cattaneo E., Ballabio A. (2009) A gene network regulating lysosomal biogenesis and function. Science. 325:473–7.

125. Settembre C., Zoncu R., Medina D.L., Vetrini F., Erdin S., Huynh T., Ferron M., Karsenty G., Vellard M.C. Facchinetti V., Sabatini D.M., Ballabio A. (2012) A lysosome-to-nucleus signalling mechanism sense and regulates the lysosome via mTOR and TFEB. EMBO J. 31, 1095-1108.

126. Martina J.A., Chen Y., Gucek M. and Puertollano R. (2012) MTORC1 functions as a transcriptional regulator of autophagy by preventing nuclear transport of TFEB. Autophagy 8, 903-914.

127. Roczniak-Ferguson A., Petit C.S., Froehlich F., Qian S., Ky J., Angarola B., Walther T.C., Ferguson S.M. (2012) The transcription factor TFEB links mTORC1 signaling to transcriptional control of lysosome homeostasis. Sci. Signal. 5, ra42.

128. Parenti G., Andria G. and Ballabio A. (2015) Lysosomal storage diseases: from pathophysiology to therapy. Annu. Rev. Med. 66, 471-486.

129. Napolitano G., Ballabio A. (2016) TFEB at a glance. J. of Cell Science 129, 2475-2481.

130. Medina D.L., Fraldi A., Bouche V., Annunziata F., Mansueto G., Spampanato C., Puri C., Pignata A., Martina J.A., Sardiello M., Palmieri M., Polishchuk R., Puertollano R, Ballabio A. (2011) Transcriptional activation of lysosomal exocytosis promotes cellular clearance. Dev. Cell 21, 421-430.

131. Spampanato C., Feeney E., Li L., Cardone M., Lim J.A., Annunziata F., Zare H., Polishchuk R., Puertollano R., Parenti G., Ballabio A., Raben N. (2013). Transcription factor EB (TFEB) is a new therapeutic target for Pompe disease. EMBO Mol. Med. 5, 691-706.

132. Song W., Wang F., Savini M., Ake A., di Ronza A., Sardiello M., Segatori L. (2013) TFEB regulates lysosomal proteostasis. Hum. Mol. Genet. 22, 1994-2009.

133. Rega L.R., Polishchuk E., Montefusco S., Napolitano G., Tozzi G., Zhang J., Bellomo F., Taranta A., Pastore A., Polishuk R., Piemonte F., Medina D.L., Catz S.D., Ballabio A., Emma F.. (2016) Activation of the transcription factor EB rescues lysosomal abnormalities in cystinotic kidney cells. Kidney Int. 89, 862-873.

134. Samson J. E., Magadan A. H., Sabri M., Moineau S. (2013) Revenge of the phages: defeating bacterial defences. Nature Rev. Microbiol. 11, 675–687.

135. Makarova K.S., Wolf Y.I., Koonin E.V. (2013) Comparative genomics of defense systems in archaea and bacteria. Nucleic Acids Res. 41, 4360–4377.

136. van der Oost J., Westra E.R., Jackson R.N., Wiedenheft B. (2014) Unravelling the structural and mechanistic basis of CRISPR–Cas systems. Nat Rev Microbiol 12(7):479-92.

137. Makarova K.S., Haft D.H., Barrangou R., Brouns S.J., Charpentier E., Horvath P., Moineau S., Mojica F.J., Wolf Y.I., Yakunin A.F., van der Oost J., Koonin E.V.

(2011) Evolution and classification of the CRISPR–Cas systems. Nature Rev. Microbiol. 9, 467–477.

138. Deltcheva E., Chylinski K., Sharma C.M., Gonzales K., Chao Y., Pirzada Z.A., Eckert M.R., Vogel J., Charpentier E. (2011) CRISPR RNA maturation by trans-encoded small RNA and host factor RNase III. Nature 471, 602–607.
139. Jinek M., Chylinski K., Fonfara I., Hauer M., Doudna J.A., Charpentier E.A. (2012) Programmable dual-RNA-guided DNA endonuclease in adaptive bacterial immunity. Science 337, 816–821.
140. Sander J.D., Joung J.K. (2014) CRIRISPR-Cas systems for editing, regulating and targeting genomes. Nat Biotechnol. 32(4):347-55.
141. Jinek M., East A., Cheng A., Lin S., Ma E., Doudna J. (2013) RNA-programmed genome editing in human cells. Elife. 29;2:e00471.
142. Ran F.A., Hsu P.D., Wright J., Agarwala V., Scott D.A., Zhang F. (2013) Genome engineering using the CRISPR-Cas9 system. Nat Protoc. 8(11):2281-308.
143. Sander J.D., Joung J.K. (2014) CRISPR-Cas systems for editing, regulating and targeting genomes. Nat Biotechnol. 32(4):347-55.
144. Saleh-Gohari N., Helleday T. (2004) Conservative homologous recombination preferentially repairs DNA double-strand breaks in the S phase of the cell cycle in human cells. Nucleic Acids Res. 32:3683–3688.
145. Cong L., Ran F.A., Cox D., Lin S., Barretto R., Habib N., Hsu P.D., Wu X., Jiang W., Marraffini L.A., Zhang F. (2013) Multiplex genome engineering using CRISPR/Cas systems. Science. 339:819– 823.
146. Qi L.S., Larson M.H., Gilbert L.A., Doudna J.A., Weissman J.S., Arkin A.P., Lim W.A. (2013) Repurposing CRISPR as an RNA-Guided Platform for Sequence-Specific Control of Gene Expression. Cell 152(5):1173-83.
147. Mali P., Yang L., Esvelt K.M., Aach J., Guell M., Dicarlo J.E., Norville J.E., Church G.M. (2013) RNA-guided human genome engineering via Cas9. Science 339:823–826.
148. Jinek M., Chylinski K., Fonfara I., Hauer M., Doudna J.A., Charpentier E. (2012) A programmable dual-RNA-guided DNA endonuclease in adaptive bacterial immunity. Science 337:816–821.
149. Zhou Y., Liu Y., Hussmann D., Brøgger P., Al-Saaidi R.A., Tan S., Lin L,. Petersen T.S., Zhou G.Q., Bross P., Aagaard L., Klein T., Rønn S.G., Pedersen H.D., Bolund L., Nielsen A.L., Sørensen C.B., Luo Y. (2016) Enhanced genome editing in mammalian cells with a modified dual-fluorescent surrogate system. Cell Mol Life Sci 73(13):2543-63.

150. Slaymaker I.M., Gao L., Zetsche B., Scott D.A., Yan W.X., Zhang F. (2016) Rationally engineered Cas9 nucleases with improved specificity. Science. 1;351(6268):84-8.
151. Mills K., Morris P., Lee P., Vellodi A., Waldek S., Young E., Winchester B. (2005) Measurement of urinary CDH and CTH by tandem mass spectrometry in patients hemizygous and heterozygous for Fabry disease. J Inherit Metab Dis. 2005;28(1):35-48.
152. Kilpatrick B.S., Eden E.R., Hockey L.N., Futter C.E., Patel S. (2015) Methods for monitoring lysosomal morphology. Methods in Cell Biology. Volume 126, Chapter 1.
153. Klionsky D.J., Elazar Z., Seglen P.O., Rubinsztein D.C. (2008) Does bafilomycin A1 block the fusion of autophagosomes with lysosomes? Autophagy 4:7, 849-850.
154. Tang W., Lu Y., Tian Q.Y., Zhang Y., Guo F.J., Liu G.Y., Syed N.M., Lai Y., Lin E.A., Kong L., Su J., Yin F., Ding A.H., Zanin-Zhorov A., Dustin M.L., Tao J., Craft J., Yin Z., Feng J.Q., Abramson S.B., Yu X.P., Liu C.J. (2011) The growth factor progranulin binds to TNF receptors and is therapeutic against inflammatory arthritis in mice. Science 332:478–484.
155. Kao A.W., Eisenhut R.J., Martens L.H., Nakamura A., Huang A., Bagley J.A., Zhou P., De L.A., Neukomm L.J., Cabello J., Farese R.V.Jr, Kenyon C. (2011) A neurodegenerative disease mutation that accelerates the clearance of apoptotic cells. Proc Natl Acad Sci U S A 108:4441–4446.
156. Seigel G.M., Wagner J., Wronska A., Campbell L., Ju W., Zhong N. (2005) Progression of early postnatal retinal pathology in a mouse model of neuronal ceroid lipofuscinosis. Eye 19, 1306–1312.
157. Hafler B.P., Klein Z.A., Jimmy Zhou Z., Strittmatter S.M. (2014) Progressive retinal degeneration and accumulation of autofluorescent lipopigments in Progranulin deficient mice. Brain Res. 1588:168-74.
158. Lieberman A.P., Puertollano R., Raben N., Slaugenhaupt S., Walkley S.U., Ballabio A. (2012) Autophagy in lysosomal storage disorders. Autophagy 8(5):719-30.
159. Yin F., Banerjee R., Thomas B., Zhou P., Qian L., Jia T., Ma X., Ma Y., Iadecola C., Beal M.F., Nathan C., Ding A. (2009) Exaggerated inflammation, impaired host defense, and neuropathology in progranulin-deficient mice. J Exp Med 207:117–128.
160. Lamb C.A., Yoshimori T., Tooze S.A. (2013) The autophagosome: origins unknown, biogenesis complex. Nat Rev Mol Cell Biol. 14(12):759-74.
161. Tanaka Y., Matsuwaki T., Yamanouchi K., Nishihara M. (2013) Increased lysosomal biogenesis in activated microglia and exacerbated neuronal damage after traumatic brain injury in progranulin-deficient mice. Neuroscience. 10;250:8-19.